Impact of Membrane Fluidity on α-syn Fibril Structures and Neuronal Pathology

Yoongyeong Baek[a], Anika Alim[b], Yanheng Dong[b], Tarek Olabi[c], Jungwoon Paek[b], Myungwoon Lee[a*]

[a] Department of Chemistry, Drexel University, Philadelphia, PA 19104

[b] Department of Electrical and Computer Engineering, Binghamton University, Binghamton, NY 13902 USA

[c] Department of Biology, Drexel University, Philadelphia, PA 19104

[*]Corresponding Author: Myungwoon Lee (ml3784@drexel.edu)

Abstract

Conformational variations in α-syn fibrils are thought to underlie the distinct clinical features of synucleinopathies, including Lewy body dementia (LBD), Parkinsons's disease (PD), and multiple system atrophy (MSA), suggesting that distinct fibril structures act as molecular fingerprints linked to disease phenotype. While the origins of these conformational variations remain unclear, increasing evidence points to membranes as key modulators of fibrils conformations. In this study, we investigated how age-related alterations in membrane composition and fluidity influence α-syn fibril formation and cellular outcomes. Using complex mixture membranes that mimic normal neuronal membranes and their age-related modifications in fatty acid chains, we found that α-syn fibrils grown with these membranes displayed distinct 2D ssNMR spectral patterns compared to lipid-free α-syn fibrils, reflecting differences in rigid fibril cores. Moreover, fibrils grown with aging-related membranes exhibited weaker membrane association than those grown with normal neuronal membranes. These membrane-associated fibrils induce stronger neuronal pathologies than lipid-free fibrils, though the severity differed in intraneuronal aggregation and inflammation responses. Overall, our findings provide new insights into how age-related changes in membrane composition shape α-syn fibril structure and pathogenicity, strengthening the link between membrane dynamics and amyloid-driven neurodegeneration.

Introduction

The aggregation of misfolded α-synuclein (α-syn), characterized by its transition from a native conformation to β-sheet-rich amyloid fibrils, constitutes the primary component of cytoplasmic inclusions known as Lewy bodies (LBs)[1,2]. These LBs are key pathological hallmarks of synucleinopathies, including Parkinson's disease (PD), Lewy body dementias (LBD), and multiple system atrophy (MSA)[3-8]. While synucleinopathies are typically classified based on clinical symptoms, the distribution of α-syn aggregates, and the affected cell types, growing research suggests that distinct α-syn fibril conformations are closely associated with specific synucleinopathies, contributing to their heterogeneous pathological features[9-13]. Nevertheless, the precise molecular mechanisms underlying α-syn fibril polymorphisms and their impact on synucleinopathy variability remain to be fully elucidated.

α-Syn fibril formation is significantly influenced by multiple factors, including α-syn concentration[14,15], temperature[16-18], and interactions with small molecules such as RNA, DNA, and lipids[19-26]. These factors have been shown to modulate the structural characteristics of α-syn fibrils. Among them, lipids are recognized as key regulators of α-syn aggregation due to their strong interactions with α-syn in both physiological and pathological contexts[22-26]. In its native state, α-syn exists as a monomer and plays a crucial role in neurotransmitter release, particularly in synaptic vesicle trafficking and fusion[27-29]. During these processes, α-syn is proposed to actively interact with various cellular membranes, such as the neuronal plasma membrane and synaptic vesicles[29,30]. However, pathological conditions may alter lipid-α-syn interactions, contributing to LB accumulation. Since LBs are composed largely of lipids together with α-syn aggregates[31], this suggests that lipid interactions may catalyze aggregation process, disrupt membrane structure, and promote co-aggregation. Consequently, lipids are now increasingly recognized as significant factors in modulating α-syn aggregation and its associated neurotoxicity.

Numerous studies have demonstrated that lipids modulate both the kinetics and conformation of α-syn fibrils[25,32-38]. For example, α-syn amyloid fibril formation is accelerated in the presence of anionic phospholipids, such as phosphatidylglycerol (PG), phosphatidylserine (PS), or phosphatidic acid (PA), at relatively low lipid-to-protein (L/P) ratios[36,38-40]. This effect is attributed to electrostatic interactions that enhance α-syn binding to membrane surfaces, thereby increasing its local α-syn monomer concentration and facilitating fibril nucleation. In contrast, binding to neutral lipid vesicles composed of phosphatidylcholine (PC) either inhibits fibril formation or has little to no effect at varying L/P ratios[37,41,42]. Beyond modulating fibril formation kinetics, membrane binding also influences the structural polymorphism of α-syn fibrils, as revealed by atomic force microscopy infrared (AFM-IR) spectroscopy, solid-state NMR (ssNMR), and cryo-electron microscopy (cryo-EM)[43-48]. Collectively, these studies highlight the critical role of lipid membranes in modulating α-syn amyloid formation.

Extensive research has focused on α-syn aggregation and its interactions with membranes, yet most studies rely on simplified membrane models containing only one or two lipid types, which fail to capture the complexity of neuronal membranes. Neuronal plasma membranes are primarily composed of multiple classes of phospholipids, cholesterol, and sphingolipids[40,49]. These complex lipid environments are critical for maintaining membrane integrity and regulating cellular functions through interactions with diverse biomolecules. However, aging disrupts the lipid balance of neuronal membranes, most notably through a decline in polyunsaturated fatty acids (PUFAs) and an increase in monounsaturated fatty acids[50-52]. Such age-related lipid alterations reduce membrane fluidity, which may, in turn, affect α-syn membrane binding affinity and aggregation behavior, potentially changing pathological processes. Despite this, the impact of fatty acid-driven changes in membrane fluidity on α-syn aggregation and its subsequent neurotoxicity remains largely unexplored. Addressing this gap requires comprehensive structural and functional studies of α-syn fibrils formed in the presence of physiologically relevant plasma membranes representing both normal and aged neurons.

In this study, we investigated how membrane composition, particularly age-related changes in fatty acid chains, affects α-syn aggregation. To this end, we developed two model membranes representing the plasma membranes of normal and aged neurons. The aged neuronal membrane was designed by modifying the lipid acyl chain length and degree of saturation of PC and phosphoethanolamine (PE) lipids—the principal phospholipids in neuronal membranes—while maintaining the same molar ratios of PC:PE:cholesterol:sphingomyelin (SM). We then characterized α-syn fibril formation in the presence of these normal and aged neuronal membranes, referred to as Neuron and Aged membranes, respectively. Our results demonstrate that both membranes facilitate fibril formation but generate distinct fibril structures with different membrane associations. Importantly, these conformational differences in α-syn fibrils drive distinct intraneuronal aggregation, neurodegeneration, and inflammatory responses, providing insights into how membrane composition contributes to the conformation-dependent pathological effects of α-syn fibrils.

Materials and Methods

Protein Expression. Recombinant full-length α-syn was expressed in *Escherichia coli (E. coli)* BL21 (DE3) competent cells. A single colony was inoculated into 10 mL of Luria-Bertani (LB) medium containing ampicillin (100 µg/ml) and incubated overnight at 37 °C with shaking at 150 rpm. The next day, the 10 mL culture was transferred into 1 L of LB medium containing ampicillin (100 µg/ml) and incubated at 37 °C with shaking at 250 rpm. Incubation continued until the optical density at 600 nm (OD_{600}) reached 0.7-0.9, at which point expression was induced with 1 mM isopropyl-β-thiogalactopyranoside (IPTG). After 4 h, cells were harvested by centrifugation at 7,000 rpm for 20 min and stored at -80 °C.

Purification of α-syn protein. The cell pellet obtained from 1 L of culture was resuspended in 25 mL of lysis buffer (10 mM Tris, pH 8, 1 mM EDTA, 1 mM PMSF, and half of Sigma Fast protease inhibitor cocktail tablet). After transferring the resuspended cells into a centrifuge tube, lysozyme (Final concentration 0.2 mg/ml) was added, and the mixture was incubated on ice for 20-30 min.

Cell lysis was performed via sonication at pulse rate of 10-sec of on-time and 15-sec of off-time, with 40% amplitude power for total on-time of 3.5 min using a Branson Digital Sonifier SFX 250. After sonication, the centrifuge tube was placed back on ice for 10-15 min before centrifuging at 16,000 rpm for 1 h at 4 °C.

To maximize purity and yield, an acid precipitation method was adapted[53]. The milky supernatant was transferred into clean 25 mL centrifuge tubes, and its pH was adjusted to 3.5. The mixture was stirred at room temperature for 20 min and then centrifuged at 16,000 rpm for 30 min at 4 °C, resulting in a clear supernatant. The pH was then adjusted back to 7.5 before an additional centrifugation step at 16,000 rpm for 1 h at 4 °C to remove aggregates.

The collected supernatant was filtered through a PVDF syringe filter with 0.45 µm pore size (Avantar, VWR® Syringe Filters) and dialyzed overnight at 4 °C against 1 L of low-salt anionic exchange buffer (10 mM Tris, pH 7.6, 25 mM NaCl, 1 mM EDTA) using a dialysis membrane with a molecular weight cutoff (MWCO) of 3.5 kDa (Spectrum Laboratories, Inc., Spectra/Por®3 Dialysis Membrane).

The following day, the dialyzed α-syn was filtered through a PES syringe filter with 0.22 µm pore size (Avantar, VWR® Syringe Filters) and loaded onto a double-stacked pre-packed HiTrap™ Q Sepharose High Performance anion exchange chromatography column (Cytiva Sweden AB, #17115401) and washed with Buffer A (10 mM Tris, pH 7.6, 25 mM NaCl, 1 mM EDTA) and Buffer B (10 mM Tris, pH 7.6, 1 M NaCl, 1 mM EDTA). α-Syn-containing fractions were pooled at conductivity of 30 mS/cm and concentrated to approximately 13 mg/ml using a 10 kDa Amicon ®Ultra centrifugal filter device (Millipore).

The concentrated protein was loaded onto a pre-packed HiPrep 16/60 Sephacryl S-200 High Resolution preparative size exclusion chromatography column (Cytiva Sweden AB, #17116601). Size exclusion

chromatography was performed in a buffer (10 mM Tris, pH 7.6, 100 mM NaCl) with a total volume of 126 ml. α-Syn protein eluted between 40 ml and 60 ml. All column chromatography was performed using an AKTA™ pure (GE Healthcare Bio-Sciences AB, Sweden). Protein concentration was determined using a NanoDrop ND-1000 UV/Vis Spectrophotometer (Thermo Fisher Scientific), and purity was assessed by SDS-PAGE gel electrophoresis. Purified α-syn was dialyzed against 1 L of distilled water overnight at 4 °C and stored at -80 °C.

Lipid Vesicle Solution. To mimic physiologically relevant normal and aged neuronal membranes, 1-palmitoyl-2-oleoyl-glycero-3-phosphocholine (POPC), 1,2-dioleoyl-sn-glycero-3-phosphoethanolamine (DOPE), 1,2-dipalmitoyl-sn-glycero-3-phosphocholine (DPPC), 1-palmitoyl-2-oleoyl-sn-glycero-3-phosphoethanolamine (POPE), cholesterol, and sphingomyelin (SM) were purchased from Avanti Polar Lipids.

The normal neuronal membrane consisted of POPC:DOPE:cholesterol:SM at molar ratios of 35:20:35:10, while the Aged membrane consisted of DPPC:POPE:cholesterol:SM at the same molar ratio. To prepare these membranes, phospholipid, cholesterol, and SM were co-dissolved in a chloroform/methanol mixture, and then the solvent was evaporated under a stream of N_2 gas. The remaining lipid film was vacuum desiccated overnight to remove residual solvent. The dried lipid films were then dissolved in 12 mM Tris-HCl buffer (pH 7.6) to a final concentration of 12.5 mM and briefly sonicated for 10-15 sec. The solution was subsequently subjected to 10 freeze-thaw cycles using liquid nitrogen and a 50 °C water bath to produce homogeneous vesicles. The resulting 12.5 mM vesicle solution was subsequently diluted to achieve the desired lipid-to-protein (L/P) ratio.

Fibril and PFFs Formation. Fibrils were generated by incubating 200 μM α-syn in 10 mM Tris-HCl buffer (pH 7.6) for four weeks at 37 °C without agitation, either in the absence or presence of lipid vesicle solutions at L:P ratios of 5, 10, and 50.

To prepare preformed fibrils (PFFs), fibrils generated with and without an L/P ratio of 10 were fragmented using a sonifier (Branson Digital Sonifier SFX 250, with Sonifier Sound Enclosure) at a pulse rate of 1-sec of on-time and 4-sec of off-time, 10% amplitude power, and total on-time of 2 min. The average length of the sonicated PFFs (~100 nm) was confirmed by negatively stained transmission electron microscopy (**Fig. S4**). The prepared PFFs were stored at -80C.

Transmission Electron Microscopy (TEM) Negatively stained samples were prepared on lacey carbon-coated copper grids (Electron Microscopy Sciences LC-325-CU-CC, Ted Pella 01824). A 10 μl aliquot of fibrils or PFFs solution was deposited onto the grid and allowed to adsorb for 1-2 min. After absorption, the solution was blotted, washed with 10 μl of water, blotted again, and stained with 10 μl of UranyLess EM stain solution (Electron Microscopy Sciences) for 30 s. TEM images were acquired on a JEOL 2100F Field-emission transmission electron microscope at 120 kV using a Gatan Ultrascan CCD camera and DigitalMicrograph (GMS3) software (Gatan Inc.).

Thioflavin T (ThT) Fluorescence Monitoring of Fibril Formation Kinetics Thioflavin-T (25 μM) was added to a freshly prepared solution of monomeric α-syn (200 μM) in the absence or presence of Neuron or Aged membranes in 10 mM Tris-HCl buffer (pH 7.6). Greiner Bio-One 96-well microplates (655900) were used for each experiment. To prevent sample dehydration during measurements, 100 μl of distilled water was added to the outermost wells. Fluorescence measurements were performed using a FLUOstar Omega (BMG LABTECH) microplate reader set to 37 °C, with excitation at 485 nm and an emission at 538 nm, monitored every 30 min or 1 h. Before each measurement, the well plate was orbitally shaken at 700 rpm for 60 sec. Experiments were conducted with three or four replicates for each sample.

Solid-State NMR (ssNMR) Sample Preparation. For ssNMR measurements, uniformly ^{13}C, ^{15}N-labeled α-syn protein was expressed in *E. coli* BL21 (DE3) competent cells. Bacteria were grown in 2 L of LB media

containing ampicillin (100 μg/ml) at 37 °C with shaking at 250 rpm until OD_{600} reached 0.5-0.6. Cells were harvested by centrifugation at 7,000 rpm for 20 min, and the pellet was resuspended in 1 L of M9 medium containing 2 g of ^{13}C-labeled glucose, 1 g of ^{15}N-labeled ammonium chloride, 2 mM of $MgSO_4$, 0.1 mM of $CaCl_2$, 100 μg/ml of ampicillin, and 10 mL of Gibco™ 100x MEM vitamin solution (Thermo Fisher Scientific). Incubation at 37 °C continued until OD_{600} = 0.8-0.9, at which point expression was induced with 1 mM IPTG. After 4 h, cells were collected by centrifugation at 7,000 rpm for 20 min and stored at -80 °C. ^{13}C and ^{15}N-labeled α-syn was purified using same procedures as for the unlabeled α-syn proteins.

Uniformly ^{13}C, ^{15}N-labeled α-syn fibrils were prepared by seeded growth. Frozen PFFs were thawed and bath-sonicated for 1 min. A 5% aliquot of the sonicated PFFs were immediately added to 200 μM of uniformly ^{13}C, ^{15}N-labeled α-syn solution to initiate fibril growth. After incubation at 37 °C, fibrils were pelleted by centrifugation at 50,000 rpm overnight at 20 °C using a Beckman SW 60Ti rotor. The pellets were slowly dried in a desiccator to achieve 55-65% water by mass. Approximately 25-30 mg of these hydrated fibrils were spun into 3.2 mm MAS rotors.

Solid-State NMR Experiments. All ssNMR experiments were conducted on an 800 MHz (18.8 Tesla) Bruker Advance III-HD NMR spectrometer equipped with a 3.2-mm ^{1}H-^{13}C-^{15}N magic angle spinning (MAS) probe (Black Fox, LLC). ^{13}C chemical shifts are reported on the TMS scale using the 38.48 ppm of CH_2 signal of adamantane. 1D ^{13}C cross-polarization (CP) and 2D ^{15}N-^{13}C and ^{13}C-^{13}C correlation spectra were measured under 13.5 kHz MAS at 275-295 K. 2D ^{13}C-^{13}C DARR spectra were acquired using mixing times of 50 ms and 100 ms[54,55].

To probe membrane association with fibrils, 2D ^{13}C-detected ^{1}H spin-diffusion spectra of α-syn fibrils grown with Neuron and Aged membranes were measured at 285-295 K under 13.5 kHz MAS[56,57]. A 400 μs ^{1}H T_2 filter was applied to suppress ^{1}H magnetization of the rigid fibrils. After ^{1}H chemical shift evolution, ^{1}H spin diffusion mixing times of 4 ms to 225 ms were used to transfer the water and lipid ^{1}H magnetization to the protein. The transferred signal was detected through ^{13}C after ^{1}H-^{13}C CP.

Calcein Release Assays. The ability of α-syn to disrupt the membrane integrity of lipid vesicles was assessed using calcein release assays, following a previously established protocol[58]. To prepare calcein-loaded lipid vesicles, freshly prepared lipid films were hydrated with 1 mL of a 100 mM calcein solution (pH 7.4) and subjected to 10 freeze-thaw cycles to facilitate calcein encapsulation. The resulting solution was extruded using a mini-extruder (Avanti Polar Lipids), passing through a 100 nm pore-size polycarbonate membrane (Cytiva) 15 times to generate a homogeneous population of unilamellar liposomes. Calcein-loaded vesicles were then separated using a gravity-flow chromatography column packed with Sephadex G-50 beads. Eluted fractions containing calcein liposomes, identified by a light orange color, were collected, while darker orange fractions, indicative of free calcein dye, were discarded. The purified calcein-containing liposomes were stored at 4 °C until use.

Fluorescence measurements were recorded every 10 min overnight using a FLUOstar Omega (BMG LABTECH) microplate reader equipped, with an excitation at 485 nm and an emission at 538 nm. All experiments were conducted at room temperature in Greiner Bio-One 96-well microplates (655900), with each well containing a total sample volume of 75 μl.

Membrane permeability was assessed by adding 13 μM of α-syn PFFs to purified calcein-containing liposomes. As a positive control for maximum dye release, calcein-containing liposomes were treated with 10% Triton X-100. Membrane permeability calculated using the following equation:

$$\text{Permeability} = 100 \times \frac{I(t) - I(t_0)}{I_{max} - I(t_0)}$$

where $I(t)$ represents the fluorescence intensity at time t, $I(t_0)$ is the initial fluorescence intensity at t=0, and I_{max} is the maximum fluorescence intensity measured after treatment with 10% Triton X-100.

Cell Culture. To establish a dopaminergic neuron model, the human neuroblastoma cell line (SH-SY5Y; ATCC, CRL-2266) was selected and expanded in 25 cm^2 flasks following the manufacturer's protocols. To culture SH-SY5Y cells, Dulbecco's Modified Eagle Medium (DMEM; 10-017-CV, Corning) was used as the basal growth medium, supplemented with 10% (v/v) heat-inactivated fetal bovine serum (hiFBS; SH30396.03, Cytiva), 1% (v/v) GlutaMAX-I (35050-06, Thermo Fisher) and 1% (v/v) penicillin-streptomycin (SV30010, Cytiva). SH-SY5Y cells at passages 3 to 10 were used as recommended by the cell supplier.

The process of dopaminergic neuronal differentiation started with trypsinization and resuspension of SH-SY5Y cells in growth medium. The harvested cells were then introduced into 48-well plates at a density of 5.0×10^5 cells/mL. The initial culture was maintained in their growth medium to promote cell adherence and stabilization. two days after seeding, the SH-SY5Y cell growth medium was replaced with the first differentiation medium consisting of DMEM supplemented with 2.5% (v/v) hiFBS, 1% (v/v) GlutaMAX-I, 1% (v/v) penicillin-streptomycin, and 10 μM retinoic acid (50-165-6969, Fisher Scientific) to induce differentiation into dopaminergic neuronal cells. After 5 days, the first differentiation medium was switched to a second differentiation medium based on Neurobasal-A (10888022, Thermo Fisher) mixed with 50 ng/mL brain-derived neurotrophic factor (BDNF; P23560, FUJIFILM Irvine Scientific), 20mM potassium chloride (KCl; 7447-40-7, Avantor Science), 1% (v/v) B27 (17-504-044, Fisher Scientific), 1% (v/v) GlutaMAX-I, and 1% (v/v) penicillin-streptomycin. The second differentiation medium was also maintained for an additional 5 days. Both the first and second differentiation media were refreshed every other day to support and sustain the dopaminergic differentiation of SH-SY5Y cells.

Treatment of PD-associated α-syn PFFs. To investigate the pathological impacts of polymorphic α-syn fibrils, our dopaminergic neuronal cells were exposed to different α-syn PFFs. For this work, a 200 μM stock solution of each α-syn PFFs conformer was sonicated for 15 sec to promote uniform dispersion and achieve an optimal working size (~100 nm). To treat dopaminergic neuronal cells, the sonicated stock solution was diluted to a final concentration of 1 μg/mL in the second differentiation medium. On Day 12 of culture, this α-syn PFFs-containing medium was added to each well containing dopaminergic neuronal cells. The cultures were then incubated with the fibrils for 72 h. After incubation, the medium was replaced with fresh differentiation medium. The treated cells were either analyzed immediately or maintained for an additional 3 days before analysis.

ThT Assay for Intraneuronal α-syn Fibrilization Analysis. To assess the extent of fibrilization induced by α-syn PFFs within dopaminergic neuronal cells, we performed a ThT assay. A 10 μM ThT working solution was prepared in DPBS. The ThT solution was then added to each well containing dopaminergic neuronal cells, followed by incubation at room temperature for 10-15 min in the dark to prevent photobleaching. After incubation, the cell cultures were washed thoroughly twice with DPBS to remove any unbound ThT. Following this, the neuronal cells in each well were imaged using an inverted fluorescence microscope (Eclipse Ti2, Nikon). To generate quantitative data, the fluorescent intensity was averaged from three samples for each experimental condition.

Immunostaining and Quantification. For immunostaining, dopaminergic neuronal cells were fixed with 4% paraformaldehyde (AR1068, Boster) for 30 min at RT and washed twice using DPBS. After fixation, cells were permeabilized with 0.1% Triton X-100 (9002-93-1, VWR) for 15 min. To prevent non-specific binding, the cells were blocked with 1.5% bovine serum albumin (BSA; 22013, Biotium) for 30 min at RT. Subsequently, the cells were incubated overnight at 4°C with primary antibodies that selectively bind to the proteins of interest.

To visualize the actin cytoskeleton, Phalloidin-CF 430 (Biotium) was applied at 1:100 dilution. Additionally, neuronal differentiation was demonstrated using primary antibodies of rabbit polyclonal anti-MAP2 (A16829, 1:200, Antibodies.com) for dendritic extensions, mouse monoclonal anti-GAP43 (A85392, 1:1000, Antibodies.com) for axonal projections, and mouse monoclonal anti-β III Tubulin (A86691, 1:500, Antibodies.com) for the neuronal cytoskeleton. To confirm PD-specific misfolding of endogenous α-syn, we used a rabbit monoclonal antibody against α-syn phosphorylated at Ser129 (A304933, 1:500, Antibodies.com). To assess the dopaminergic characteristics of neuronal cells, Tyrosine Hydroxylase (TH) expression was examined using a mouse monoclonal anti-TH antibody (A104316, 1:5000, Antibodies.com). For investigating inflammatory responses, we used a rabbit polyclonal anti-NF-kB antibody (51-0500, 1:500, ThermoFisher).

After incubation with primary antibodies, cells were washed twice with DPBS and incubated for 1-2 hours at RT with fluorescently labeled secondary antibodies (A32732, ThermoFisher; A32723, ThermoFisher; A32731, ThermoFisher; A11032, ThermoFisher). We also used Hoechst (33342, ThermoFisher) for nuclear staining.

Finally, fluorescence images of the cells were captured using the Nikon Ti2-Eclipse microscope, and image processing was performed using NIS Elements software. To quantitively assess the data, fluorescent intensity was averaged from 3 samples for each experimental condition.

Statistical analysis. Statistical value of the obtained data was assessed by a two-tailed t-test. Results from three independent experiments are presented as mean ± SD.

RESULTS

α-syn Forms Fibrils in the Presence of Normal and Aged Neuronal Membranes.

To investigate the membrane-dependent conformational changes of α-syn fibrils, 200 μM of α-syn monomers were incubated at 37 °C with and without lipid vesicles at a lipid-to-protein (L/P) ratio of 10, under quiescent conditions. To model the physiological conditions of neuronal membranes and their age-related alterations, we prepared two types of vesicles: Neuron membranes, representing normal neuronal plasma membranes, and Aged neuronal membranes. Neuron membranes were composed of 1-palmitoyl-2-oleoyl-glycero-3-phosphocholine (POPC), 1,2-dioleoyl-sn-glycero-3-phosphoethanolamine (DOPE), cholesterol, and sphingomyelin (SM) at a 35:20:35:10 molar ratio. To reflect the reduction in unsaturated fatty acid chains observed in brains with aging, Aged membranes were prepared by substituting POPC and DOPE with 1,2-dipalmitoyl-sn-glycero-3-phosphocholine (DPPC) and 1-palmitoyl-2-oleoyl-sn-glycero-3-phosphoethanolamine (POPE), while maintaining the same molar ratios (**Fig. 1**). Fibril formation, in both the absence and presence of membranes, was confirmed by negatively stained transmission electron microscopy (TEM) (**Fig. 2A-C**).

Structural changes in α-syn monomers during incubation were monitored by circular dichroism (CD) spectroscopy (**Fig. 2D**). Initially, α-syn monomers incubated with Neuron (green) or Aged (red) membranes exhibited α-helical-like spectra, characterized by two minima near 208 and 222 nm, consistent with previous reports that membrane-bound α-syn adopts a helical structure[59-61]. After 400 hours of incubation without agitation, a pronounced negative peak appeared near 218 nm, indicating a transition to a β-sheet-rich conformation, a hallmark of fibril formation. These results confirm that α-syn monomers forms fibrils over extended incubation periods in the presence of both model membranes.

The presence of membranes alters a-syn Aggregation Kinetics.

Thioflavin T (ThT) fluorescence assays were used to monitor the aggregation kinetics of α-syn under varying protein concentrations and L/P ratios (**Fig. 3A-C**). The $t_{0.1}$ and $t_{0.5}$ values – corresponding to the

times required to reach 10% and 50% of maximal ThT fluorescence intensity, respectively – were used to quantitatively compare aggregation properties under different conditions (**Fig. 3D**). These values are commonly referred to as the lag phase and elongation phase, reflecting monomer nucleation and subsequent conversion into amyloid forms, respectively[20]. In the absence of lipids, accelerated fibril formation was observed at higher α-syn monomer concentrations, as indicated by reduced $t_{0.1}$ and $t_{0.5}$ values (**Fig. 3A**). To assess the effects of Neuron and Aged membranes on fibril formation, all subsequent experiments were conducted at a monomer concentration of 200 μM with L/P ratios of 5, 10, and 50 (**Fig. 3B, C**).

The presence of both Neuron and Aged membranes enhanced α-syn fibril formation across all L/P ratios. With Neuron membranes (**Fig. 3B**), increasing the L/P ratio from 5 to 10 reduced the lag time and steepened the sigmoidal curve, reflecting more efficient nucleation and elongation process. However, at an L/P ratio of 50, fibril formation slowed to a rate similar to that observed at an L/P ratio of 5. We attribute this effect to membrane surface-bound α-syn, which acts as a nucleation site, promoting aggregation at relatively low L/P ratios. However, as more α-syn binds to lipid vesicles at an L/P ratio of 50, the concentration of free α-syn monomers in solution decreases, slowing fibril formation. In contrast, in the presence of Aged membranes (**Fig. 3C**), the greatest acceleration in fibril formation was observed at an L/P ratio of 50. This suggests that α-syn has a lower binding affinity for Aged membranes compared to Neuron membranes, allowing a higher concentration of free α-syn to remain in solution, thereby facilitating fibril formation at an L/P ratio of 50.

Membrane-Induced Conformational Variations in α-syn Fibrils Revealed by Solid-State NMR.

To better understand how membrane environments influence α-syn fibril conformations, we measured 2D ^{15}N-^{13}C correlation spectra of α-syn fibrils formed either without lipids or in the presence of Neuron or Aged membranes at an L/P ratio of 10 (**Fig. 4A-C**). Measurements were conducted under conditions optimized for ssNMR, using cross-polarization (CP) driven by dipolar coupling-based polarization transfer, to detect signals from the immobilized rigid fibril core. In the 2D ^{15}N-^{13}C spectra, all three fibril samples exhibited most peaks with ^{15}N chemical shifts exceeding 120 ppm, indicating β-sheet conformations. Distinct peaks, highlighted by cyan circles, confirm membrane-induced conformational variations among the three fibrils.

To obtain amino acid-specific structural information of the fibril core, we measured 2D ^{13}C-^{13}C correlation spectra using a dipolar coupling-based polarization transfer sequence. The 2D ^{13}C-^{13}C correlation spectrum of lipid-free α-syn fibrils, acquired with a 100 ms DARR mixing time, shows β-sheet chemical shifts for Thr, Val/Pro, Gln/Glu/Lys, and Ala residues, along with a small helical Thr peak and random coil peaks for Ala and Gln/Glu/Lys residues. This confirms that lipid-free α-syn fibrils adopt a β-sheet rich amyloid structure with a small, disordered region (**Fig. 4A**). The 2D ^{13}C-^{13}C correlation spectra of α-syn fibrils grown with Neuron or Aged membranes show predominant peaks that align closely with those observed in lipid-free fibrils (**Fig. 4B, C**). However, these membrane-associated fibrils lack the α-helical Thr peak observed in lipid-free fibrils and instead exhibit additional β-sheet Thr peaks, indicating conformational changes in the fibril core. Notably, fibrils grown with Neuron or Aged membranes display inter-residue cross peaks between Thr-Ala or Thr-Lys, despite being measured with a shorter 50 ms DARR mixing time compared to lipid-free fibrils. This observation suggests that membrane-associated fibrils adopt a more compact and rigid core structure. Considering the multiple Thr-Lys and Thr-Ala pairs in the α-syn sequence, these inter-residue correlations likely result from intra-molecular interactions.

To quantitatively compare the relative abundance of amino acids within the rigid α-syn fibril core, we measured the intensities of Cα-Cβ cross peaks for Val/Pro, Ala, Thr, Gln/Glu, and Gln/Glu/Lys residues in each 2D ^{13}C-^{13}C correlation spectrum. The peak intensities were then normalized to the total sum of these selected peaks (**Fig. 4D**). Because dipolar coupling-based 2D ^{13}C-^{13}C correlation experiment detects signals from rigid fibril cores, the normalized peak intensities provide a quantitative estimate of the relative number

of amino acids within the fibril core. Therefore, differences in amino acid intensity ratios among the three fibrils indicate that each fibril has a unique fibril core, comprising different segments of the α-syn sequence, supporting membrane composition-dependent structural variations. As shown in **Fig. 4D**, the fibril core of lipid-free α-syn contains more than 30% of Gln, Glu, and Lys residues, while Thr accounts for only about 11%. In contrast, α-syn fibrils grown with Neuron membranes contain approximately 28% Val and Pro residues, with the lowest proportion (~12%) of Gln and Glu residues. The amino acids composition of α-syn fibrils formed in the presence of Aged membranes resembles that of lipid-free α-syn fibrils but with an increased Thr content. The 1D ^{13}C CP spectra of the three fibrils also exhibit consistent variations in peak intensity (**Fig. 4E**). In lipid-free α-syn fibrils, the spectrum shows stronger signals for Gln/Glu/Lys residues in the 52-55 ppm range and weaker Thr peaks in the 66-69 ppm range compared to the two membrane-associated fibrils. These observations align with the calculated peak intensities from the 2D ^{13}C-^{13}C correlation spectra (**Fig. 4E**).

We further utilized normalized peak intensities to estimate the fibril core sequence by comparing relative peak intensities with the number of amino acids in specific regions of the α-syn sequence. For example, the normalized peak intensities of lipid-free fibrils closely match the relative number of amino acids in the α-syn sequence from residue M1 to Q100, suggesting that lipid-free fibrils primarily comprise the N-terminal 100 residues of α-syn (**Fig. S2B,C**). In contrast, α-syn fibrils grown with Neuron or Aged membranes exhibit normalized peak intensities corresponding to sequences spanning residues V38-F95 and E14-Q100, respectively (**Fig. S2D-2G**). These results indicate that membrane presence and its composition influence the conformation of α-syn fibrils. However, further structural analysis is necessary to precisely define the fibril core regions and characterize membrane-induced structural changes.

Distinct Membrane Contacts of α-syn Fibrils with Neuron and Aged Membranes.

To investigate the molecular contacts between α-syn fibrils and membranes, we performed 2D ^{13}C-detected ^{1}H-^{1}H spin diffusion NMR experiments on α-syn fibrils grown with Neuron or Aged membranes at an L/P ratio of 10. This experiment correlates the ^{1}H signals from water or lipid acyl chains with ^{13}C signals from the protein by selectively transferring water and lipid ^{1}H signals to the ^{13}C-labeled protein using a 400 μs T_2 filter, followed by varying ^{1}H-^{1}H spin diffusion mixing times ranging from 4 to 225 ms. The extent of fibril-membrane and fibril-water interactions can be assessed by comparing the intensities of protein signals transferred from lipids and water.

Fig. 5A and **5C** show representative 2D ^{1}H-^{13}C spectra of α-syn fibrils grown with Neuron and Aged membranes, respectively, measured with a 100 ms of ^{1}H-^{1}H mixing time. In both cases, cross peaks with the lipid acyl chain CH_2 signal at 1.3 ppm and CH_3 signal at 0.9 ppm are observed, indicating that both fibrils contact the membranes. Notably, α-syn fibrils grown with Neuron membranes exhibited stronger protein signals transferred from lipids compared to those grown with Aged membranes, implying stronger membrane interactions in the former.

To quantitatively compare the membrane association of the two fibrils, we extracted 1D cross-sections of ^{13}C protein signals transferred from lipid CH_2 (1.3 ppm) and water (5.0 ppm) in the 2D spectra measured with ^{1}H mixing times of 4 ms and 100 ms and compared their intensities. At a 4 ms mixing time, both fibrils show a lipid-to-protein cross peak intensity of approximately 6-7% relative to the water-to-protein cross peak intensity (**Fig. 5B** and **5D**). This ratio is below the typical range observed for membrane-spanning proteins (10-25%)[62-64], suggesting that neither fibril is deeply embedded into the membrane bilayer. At a 100 ms of ^{1}H mixing time, α-syn fibrils grown with Neuron membranes maintain a similar ~7% lipid-to-protein cross peak intensity relative to water-to-protein cross peaks, indicating that both lipid and water signals increase proportionally with longer ^{1}H-^{1}H spin diffusion mixing times. In contrast, α-syn fibrils grown with Aged membranes show a significant increase in water-to-protein cross peak intensity but not in lipid-to-protein intensity at a 100 ms ^{1}H mixing time, reducing the lipid-to-water cross peak intensity

ratio to 1.6%. This suggests that water signal transfer dominates over lipid signal transfer at longer mixing times, implying that α-syn fibrils grown with Aged membranes engage in weaker membrane interactions than those grown with Neuron membranes. **Fig. 5E** presents the lipid-to-protein and water-to-protein ^{1}H polarization transfer curves for both fibrils as a function of ^{1}H spin diffusion mixing time. The intensities at each ^{1}H mixing time were normalized to the maximum water-to-protein intensity at 100 ms. The resulting plots reveal that protein signals transferred from Aged membranes plateaued after 25 ms of ^{1}H mixing time, whereas those from Neuron membranes continued to increase. Additionally, the lipid-to-protein signal intensity for α-syn fibrils associated with Aged membrane is significantly lower, approximately three times less, than for fibrils with Neuron membranes. The significantly weak and rapidly saturated lipid-to-protein signals for α-syn fibrils grown with Aged membranes implies that α-syn fibril insertion into the Aged membrane bilayer is limited to a subset of fibrils, or that some broken membrane fragments are incorporated into the fibrils. By contrast, α-syn fibrils grown with Neuron membranes display a steady increase in lipid-to-protein signal intensity up to 225 ms (Data not shown), indicating that these fibrils not only insert into the lipid bilayer but also remain associated with surrounding Neuron vesicles.

Conformation-Dependent Intraneuronal Aggregation Properties and Inflammatory Responses.

To test whether membrane-derived conformations drive distinct neuronal pathologies, we generated forms of pre-formed fibrils (PFFs) by sonicating α-syn fibrils grown without membrane, with Neuron membranes, or with Aged membranes. The resulting fibril segments, approximately 100 nm in length as confirmed by negatively stained TEM (**Fig. S5**), are referred to as PFFs, N-PFFs, and Aged-PFFs, respectively.

To evaluate the conformation-dependent prion-like behavior, we applied 0.4% of PFFs, N-PFFs, or Aged-PFFs to a 200 μM solution of monomeric α-syn and monitored fibril formation by ThT fluorescence. Aggregation kinetics were quantified using $T_{1/10}$ and $T_{1/2}$. All types of PFFs significantly accelerated fibril formation, with Aged-PFFs exhibiting the most pronounced effect, as indicated by their shortest $T_{1/10}$ and $T_{1/2}$ values (**Fig. S7**). These findings support conformation-dependent variations in the prion-like characteristics of fibrils.

In the next phase of our study, we examined how these polymorphic α-syn fibrils shape disease-relevant phenotypes in dopaminergic neurons, the cell type most affected in PD[65-67]. To this end, we established an in vitro model of midbrain neuronal tissue by differentiating neuroblastoma cells, which are commonly employed as a dopaminergic cell model in PD research[68-70]. Specifically, neuroblastoma cells were introduced into 48-well plates and cultured until reaching confluency (**Fig. S7A**). Neuronal differentiation was then initiated through sequential application of two defined media formulations designed to drive morphological maturation as previously established[71,72] (**Fig. S7B**). During the early phase of differentiation (Day 2), cells began to extend thin projections (**Fig. S7C, Day 4**), which progressively developed into a dense network of neurite-like structures by Day 12 (**Fig. S7C, Day 12**). Following differentiation, the cells were evaluated for neuronal features by immunostaining for dendritic and axonal markers. This analysis revealed robust expression of microtubule-associated protein 2 (MAP2) and growth-associated protein 43 (GAP43), which serve as markers for dendrites and axons, respectively, confirming that the differentiated neuroblastoma cells had acquired characteristic neuronal phenotypes[73-77] (**Fig. S7D**). Their dopaminergic identity was also validated by immunofluorescent staining for tyrosine hydroxylase (TH), an enzyme essential for dopamine biosynthesis and a well-established marker of midbrain dopaminergic neurons[78,79] (**Fig. S7D)**.

Building on this neuronal platform, we next investigated how dopaminergic neurons respond to conformationally distinct α-syn PFFs. Specifically, our dopaminergic neuronal cells were treated with PFFs, N-PFFs, and Aged-PFFs to induce pathological features characteristic of PD, while α-syn monomers and untreated cultures served as controls. A concentration of 1.0 μM was used for all α-syn species, consistent with prior studies showing that concentrations between 0.25 and 2.0 μM effectively induce PD-associated pathologies in neuronal cultures without causing acute toxicity[80-86]. After 3 days of treatment, we first

examined whether the polymorphic α-syn PFFs differed in their ability to induce de novo formation of protein aggregates, a pathological hallmark of PD. To assess this, we used ThT, a fluorescent dye commonly used to probe intracellular protein fibrils[87]. As a result of this assay, we observed that both N-PFF and Aged-PFF treatments significantly increased ThT fluorescence intensity in dopaminergic neuronal cells compared to other conditions, indicating enhanced intraneuronal aggregation (**Fig. 6A**). As shown in **Fig. 6B**, our quantitative analysis further confirmed this observation, showing that N-PFFs led to a 2.5-fold increase and Aged-PFFs a 2-fold increase in ThT signal compared to the untreated control. In contrast, PFFs showed only a nonsignificant trend toward increased aggregation, and α-syn monomers failed to induce detectable fibril formation (**Fig. 6A, B**). These findings indicate that N-PFFs and Aged-PFFs, but not PFFs or monomers, effectively seed intraneuronal aggregation in our dopaminergic neuronal cells.

In the subsequent phase of the study, we evaluated whether distinct conformations of α-syn PFFs differentially triggered inflammatory responses in our neuronal cells, given increasing evidence that α-syn aggregates contribute to neuroinflammation associated with PD progression[88-90]. As a representative readout of neuroinflammatory activation, we analyzed the subcellular localization of nuclear factor-kappa B (NF-κB), a key transcription factor involved in inflammation and cellular stress responses[91,92]. In the absence of pathogenic PFFs, as in untreated and monomer-treated cultures, NF-κB was largely retained in the cytoplasm (**Fig. 6C**), consistent with its inactive state under non-inflammatory conditions. Exposure to N-PFFs or Aged-PFFs, however, induced robust NF-κB nuclear translocation, as evidenced by increased nuclear and decreased cytoplasmic staining (**Fig. 6C**). Quantitative analysis also revealed approximately a 1.5-fold increase in NF-κB nuclear translocation in cultures treated with N-PFFs and Aged-PFFs compared to untreated controls and α-syn monomer-treated cells (**Fig. 6D**). It should be noted that treatment with PFFs did not alter NF-κB distribution, indicating the conformational specificity of the inflammatory response.

Finally, we investigated whether distinct α-syn PFF polymorphs led to variation in post-translational modification of α-syn, a hallmark of synucleinopathy progression. Specifically, we assessed phosphorylation at serine-129 (pS129), the predominant post-translational modification enriched in PD Lewy bodies[93-95]. Treatment with N-PFFs and Aged-PFFs significantly increased the immunofluorescence intensity of pS129 α-syn in dopaminergic neuronal cells, with quantification showing more than a 2-fold increase compared to control and monomer-treated groups (**Fig. 6E, F**). PFFs again failed to induce a significant increase in pS129 α-syn immunofluorescence intensity in comparison to that observed in control groups. While further studies are needed, these observations implicate specific α-syn fibril structures in driving pathogenic serine-129 phosphorylation.

Collectively, these in vitro study results show that N-PFFs and Aged-PFFs, but not PFFs or monomeric α-syn, trigger key pathological features of PD, including intracellular fibril aggregation, NF-κB-mediated neuroinflammation, and abnormal α-syn phosphorylation. This suggests that structural variation among α-syn fibril conformers may play a critical role in modulating neuroinflammatory responses as well as protein misfolding and aggregation, key contributors to dopaminergic neurodegeneration in PD.

Discussion

α-syn membrane binding has been recognized as a critical step in its pathological role, primarily by nucleating aggregation[36,96]. To date, extensive studies have examined how lipids—particularly headgroup composition—affect α-syn aggregation kinetics, largely using simplified membranes composed of one or two lipid types [25,35-38,40,45]. However, the influence of lipid fatty acid composition, which primarily governs membrane fluidity and packing, on α-syn aggregation within physiologically relevant neuronal membranes remains underexplored. Notably, aging is associated with a decrease in PUFAs and an increase in

monounsaturated fatty acids, representing major alterations in brain lipid composition that reduce membrane fluidity and dynamics[50-52].

Here, we provide important insights into how these age-related alterations in membranes influence α-syn fibril formation and pathology using two neuronal membrane models that recapitulate normal and aged lipid compositions. Our results showed that the two membranes affected fibril cores differently, producing distinct membrane association. Specifically, α-syn fibrils formed with Aged membranes exhibit weaker membrane association compared to those formed with Neuron membranes. To verify that this weaker interaction was not due to the relatively low L/P ratio of 10, we performed the 2D ^{13}C detected ^{1}H-^{1}H spin diffusion experiments on α-syn fibrils grown with Aged membranes at an L/P ratio of 50. The lipid-to-protein signal intensity was comparable to that observed at an L/P ratio of 10 (**Fig. S3**), confirming that the reduced lipid-to-protein signals reflect intrinsically weak membrane association in Aged membranes.

Although both membranes are composed of zwitterionic lipids lacking charged species known to strongly influence α-syn binding affinity, lipid packing defects also play an important role. These defects, defined as transient surface gaps between lipid headgroups that expose underlying hydrophobic fatty acid chains to solvent[97], have been shown to enhance α-syn membrane binding[98,99]. The extent of lipid packing defects, quantified as the exposed hydrophobic area of lipid bilayers due to non-ideal packing, increases with the degree of fatty acid unsaturation[100]. Thus, the enhanced membrane binding of α-syn to Neuron membranes, which contain more unsaturated lipids (POPC and DOPE) compared to Aged membranes (DPPC and POPE), can be attributed to the higher level of lipid packing defects in Neuron membranes. These lipid packing defects promote hydrophobic interactions that facilitate α-syn insertion into the membrane bilayer[101]. Consistent with this, our study showed stronger lipid interactions with hydrophobic residues (Val, Ala, and Gly) than with hydrophilic residues (Gln, Glu, Lys, and Thr) in α-syn fibrils grown with Neuron membranes (**Fig. S4C**), suggesting that hydrophobic resides are more deeply inserted into the bilayer. In contrast, fibrils grown with Aged membranes showed similar levels of lipid interactions across both hydrophobic and hydrophilic residues (**Fig. S4E**), implying that the α-syn sequence is only superficially embedded at the membrane surfaces, with weaker hydrophobic contacts between lipid acyl chains and α-syn.

These distinct membrane interactions may give rise to different fibril structures. Although thorough comparisons will require the development of structural models for each fibril, our ssNMR data suggest that the fibril cores span residues 38-95 for α-syn fibrils grown with Neuron membranes and residues 14-100 for those grown with Aged membranes (**Fig. S2**). This indicates that fibrils formed with Neuron membranes retain a longer N-terminal disordered region (residues from 1-37) than those formed with Aged membranes. Because the N-terminal region is known to mediate membrane binding[61,102-104], its stronger affinity for Neuron membranes likely promotes insertion of a longer portion of this region into the lipid bilayer. This insertion may limit its involvement in fibril core formation through protein-protein hydrophobic interactions, resulting in a longer disordered segment compared to fibrils grown with Aged membranes.

In an attempt to translate membrane-associated α-syn conformers into a patho-physiologically relevant context, we employed an in vitro cell-based platform to investigate the pathological consequences of α-syn polymorphism. Building upon this interdisciplinary strategy, we found that distinct α-syn PFF conformations elicited differential responses in dopaminergic neuronal cells across multiple pathological processes implicated in PD neurodegeneration. Notably, α-syn PFFs prepared from lipid-free fibrils, widely used to study intracellular aggregates and PD pathologies in cell and animal models[11,105,106], failed to produce pathological effects comparable to those of N-PFFs and Aged-PFFs in our dopaminergic neuronal cells. Although further investigation is required, we attribute this discrepancy to differences in fibril growth conditions that may alter fibril the structure properties of PFFs. In prior studies, most lipid-free PFFs were generated under shaking conditions and were shown to form central fibril cores with N-terminal disordered segments[107-109]. In contrast, lipid-free PFFs produced in this study without agitation formed a fibril core

lacking N-terminal disorder, suggesting a critical role of the N-terminal region in driving pathogenic effects. Consistent with this, both membrane-associated PFFs exhibited pronounced neuronal pathologies, and these fibrils are predicted to possess disordered N-terminal regions spanning residues 1-37 and 14-100, respectively (**Fig. S2**). In support of this, membrane permeability assays showed that N-PFFs induced the strongest membrane permeability, followed by Aged-PFFs and PFFs (**Fig. S6**), suggesting that N-PFFs exert the greatest destabilizing effect. Collectively, these findings suggest that the flexible N-terminal region may contribute to the pathological processes by interacting with cellular membranes or facilitating monomer recruitment.

In our dopaminergic neuronal cells, the two membrane-associated PFFs also displayed distinct pathological features, differing in both seeding capacity and inflammatory response. Notably, Aged-PFFs induced greater NF-κB nuclear translocation than N-PFFs (**Fig. 6C, D**), despite seeding less intraneuronal aggregation (**Fig. 6A, B**).

Taken together, our observations support the idea that structural diversity among α-syn fibrils contributes to phenotypic heterogeneity across synucleinopathies, in agreement with previous reports implicating α-syn polymorphism in the variability observed among these disorders[10,110,111].

While our in vitro dopaminergic neuronal model recapitulates several hallmark features of PD pathology, it remains an incomplete representation of the functional complexity of in vivo dopaminergic neurons. In particular, the absence of validated synaptic connectivity may limit its ability to capture interneuronal transmission of α-syn species, a process thought to play a pivotal role in disease progression[112-114]. This limitation constrains the extent to which the cellular model can be used to investigate disease mechanisms, as it does not account for the interneuronal spread of pathogenic α-syn, an important aspect of disease progression. To improve the translational relevance of this cellular model, future efforts will need to demonstrate reliable formation of synaptic structures and the occurrence of action potential-mediated synaptic transmission.

Conclusion

In conclusion, our study demonstrates that complex membranes, containing cholesterol, phospholipids, and sphingolipids, which mimic neuronal plasma membranes, accelerate α-syn aggregation and generate fibril structures distinct from those formed without membranes. ssNMR data further reveal that age-associated changes in phospholipid fatty acid chains alter both the structures and aggregation kinetics of α-syn fibrils, leading to distinct modes of membrane-association. Moreover, the differences in intraneuronal aggregation and inflammatory responses induced by distinct forms of PFFs, highlight the critical role of membrane fluidity and fatty acid composition in shaping pathogenic protein aggregation. Together, these findings advance our understanding of conformation-dependent pathologies and provide insights into the interplay between neurodegenerative aggregates and aging.

Author Contributions

M.L and J.P designed the project. Y.B, A.A, Y.D and T.O performed experiments. M.L, J.P, Y.B, and A.A wrote the manuscript.

Acknowledgements

We thank Drs. Ivan Hung and Zhehong Gan at the National High Magnetic Field Laboratory for their assistance with ssNMR experiments. The National High Magnetic Field Laboratory is supported by the National Science Foundation through NSF/DMR-2128556 and the state of Florida.

This work was supported by NIH grant NS139178 to M.L and J.P.

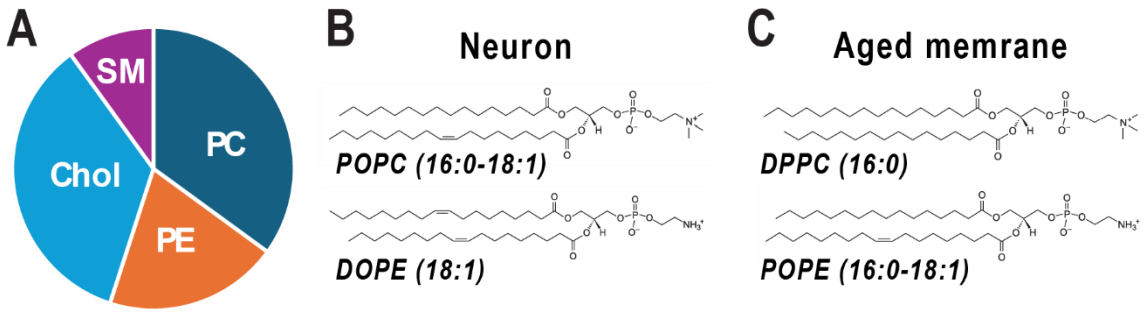

Figure 1. Lipid compositions of model membranes mimicking plasma membranes of normal and aged neurons, referred to as Neuron and Aged membranes in this study. (A) Lipid compositions of Neuron and Aged membranes, consisting of PC, PE, Cholesterol, and SM in a 35:20:35:10 molar ratio. (B) Chemical structures of POPC and DOPE, the primarily lipid components of the Neuron membrane. (C) Chemical structures of DPPC and POPE, which characterize the Aged membrane with altered saturation levels. Compared to POPC and DOPE in Neuron membranes, DPPC and POPE have shorter and more saturated acyl chains.

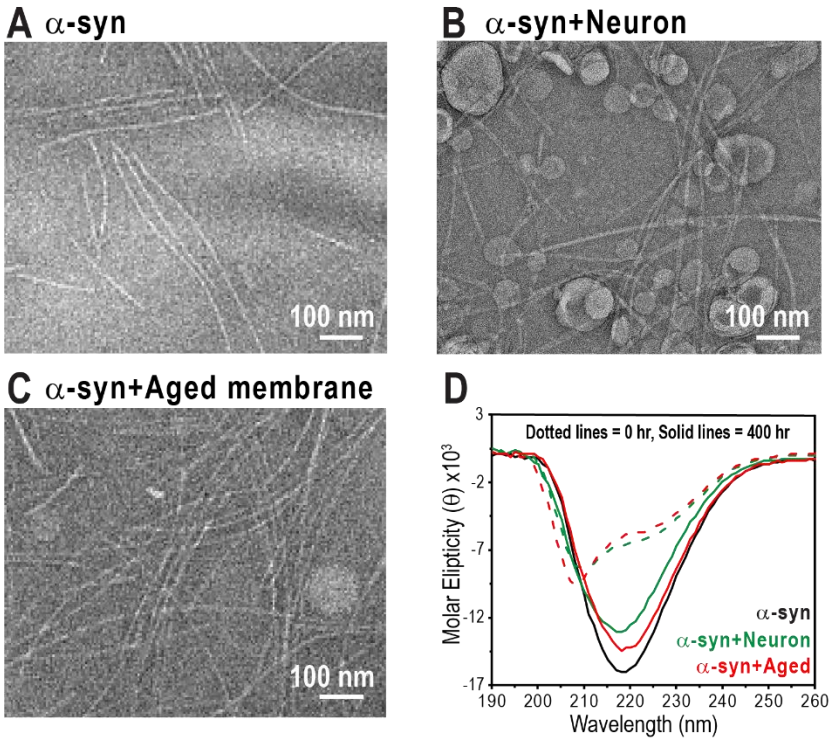

Figure 2. Characterization of α-syn fibril formation in the absence and presence of lipid membranes. (A-C) Negatively stained TEM images confirming fibril formation after incubation: (A) α-syn fibrils without membranes, (B) α-syn fibrils formed in the presence of Neuron membrane, and (C) α-syn fibrils formed in the presence of Aged membranes. Scale bars represent 100 nm. (D) CD spectra of α-syn in the absence (black) and presence of Neuron (green) or Aged membrane (red) over 400 hours of incubation without agitation. Dotted lines represent spectra at 0 hours, while solid lines indicate spectra at 400 hours, revealing structural transitions from an α-helical to a β-sheet-rich fibril conformation.

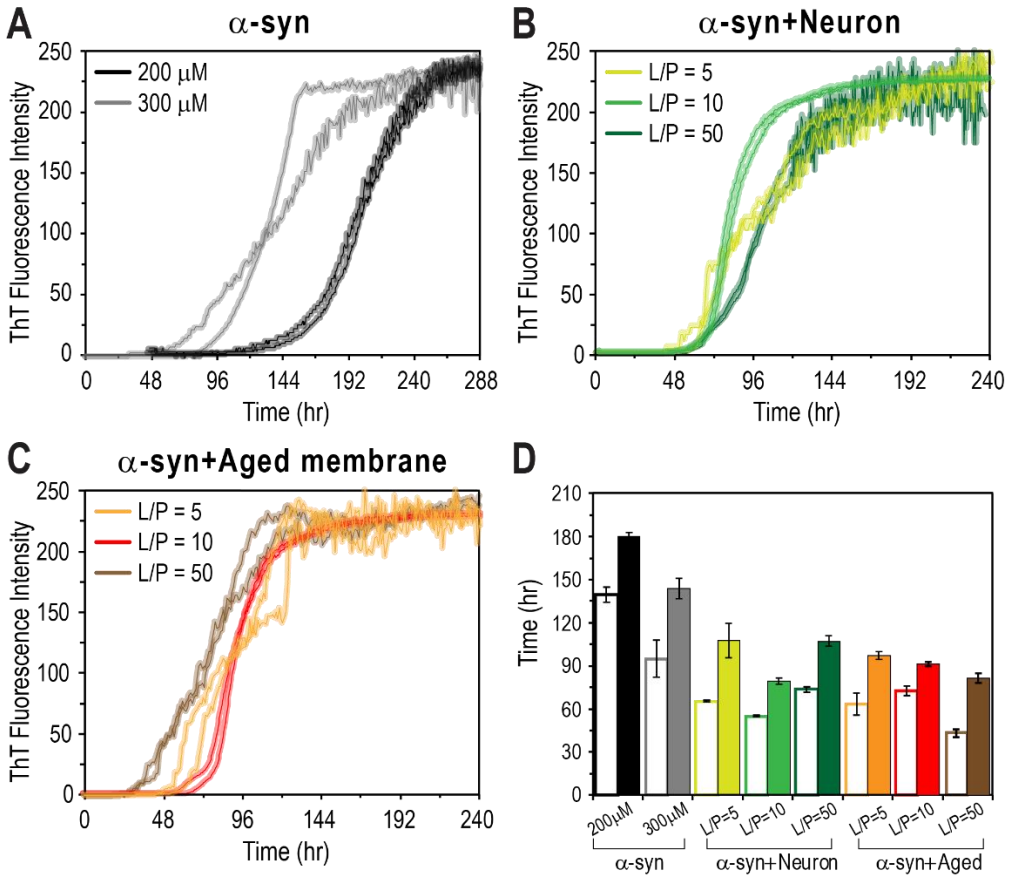

Figure 3. Effects of protein concentration and L/P ratio on α-syn aggregation kinetics. (A) ThT fluorescence curves of α-syn aggregation kinetics at monomer concentration of 200 μM (black) and 300 μM (gray) in the absence of lipid over 288 hours. Higher α-syn concentrations result in shorter lag times and steeper sigmoidal curves. (B) ThT fluorescence curves of α-syn aggregation in the presence of Neuron membranes at L/P ratios of 5 (lime green), 10 (green), and 50 (dark green) over 240 hours. Aggregation is enhanced as the L/P ratio increases from 5 to 10, whereas fibril formation slows at an L/P ratio of 50 due to α-syn sequestration on lipid vesicles. (C) ThT fluorescence curves of α-syn aggregation in the presence of Aged membranes at L/P ratios of 5 (orange), 10 (red), and 50 (brown) over 240 hours. Unlike Neuron membranes, Aged membranes exhibit the shortest lag time at an L/P ratio of 50, suggesting a lower α-syn binding affinity. (D) Quantitative comparison of aggregation kinetics using $t_{0.1}$ (open bars) and $t_{0.5}$ (solid bars), representing the times required to reach 10% and 50% of maximal ThT fluorescence intensity, respectively. The same color scheme from (A-C) is applied.

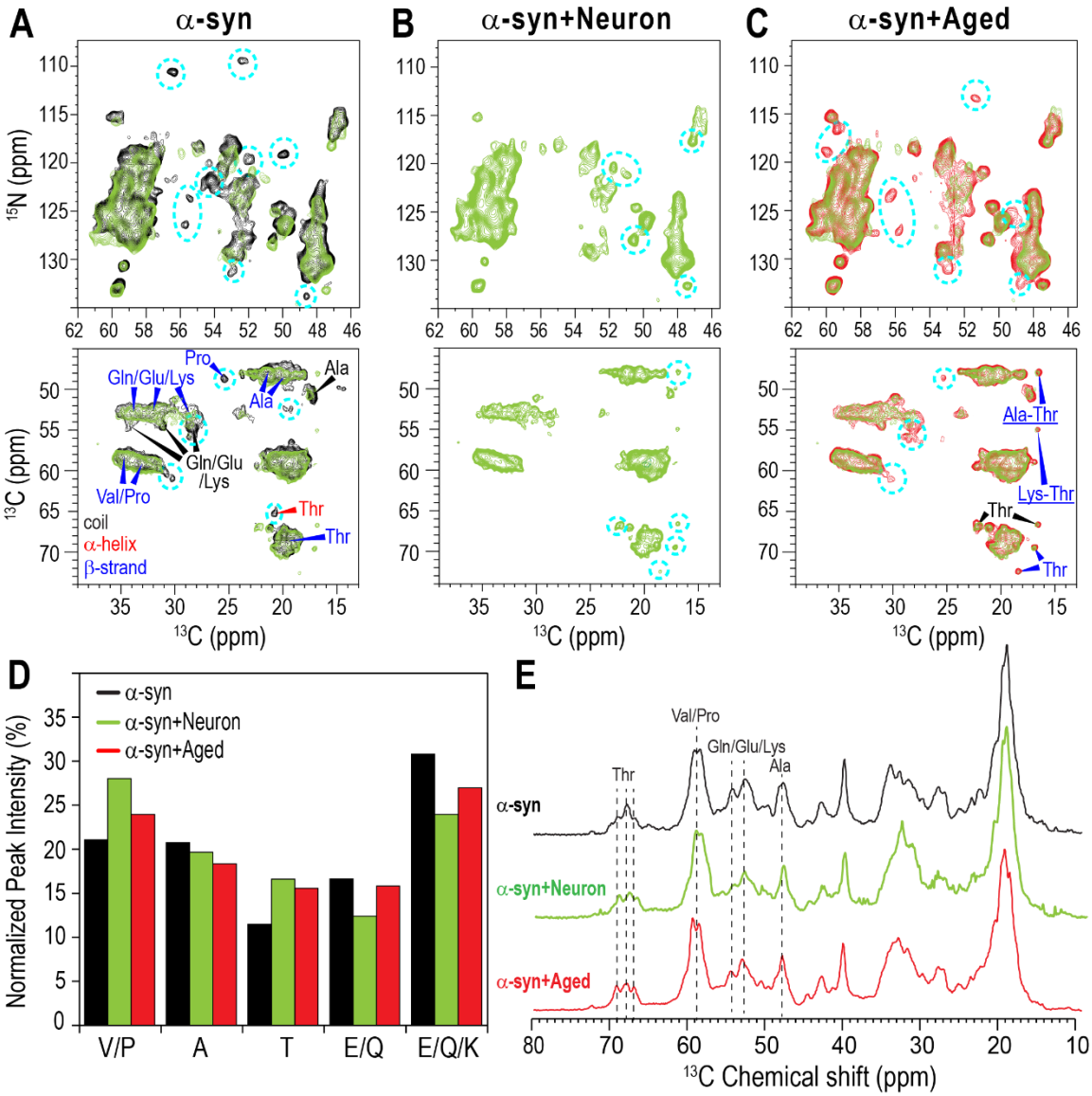

Figure 4. Comparison of 2D NMR spectra of α-syn fibrils grown under different conditions. (A) 2D ^{15}N-^{13}C (top) and ^{13}C-^{13}C correlation spectra (bottom) of lipid-free α-syn fibrils (black) overlaid with the α-syn fibrils grown with Neuron membranes (green). (B) 2D ^{15}N-^{13}C (top) and ^{13}C-^{13}C correlation spectra (bottom) of α-syn fibrils grown with Neuron membranes (green). (C) 2D ^{15}N-^{13}C (top) and ^{13}C-^{13}C correlation spectra (bottom) of α-syn fibrils formed with Aged membranes (red), overlaid with α-syn fibrils grown with Neuron membranes (green). Cyan circles highlight distinct peaks indicating membrane-induced conformational variations. (D) Quantification of relative amino acid composition within the fibril core based on normalized Cα-Cβ cross peak intensities from 2D ^{13}C-^{13}C spectra, showing differences among lipid-free (black), Neuron (green), and Aged (red) membrane-associated α-syn fibrils. (E) 1D ^{13}C CP spectra of the three fibril types grown in lipid-free conditions (black), with Neuron membranes (green), and with Aged membranes (red). Labeled peaks in the 1D spectra correspond to those in the 2D ^{13}C-^{13}C spectra used for intensity quantification in (D).

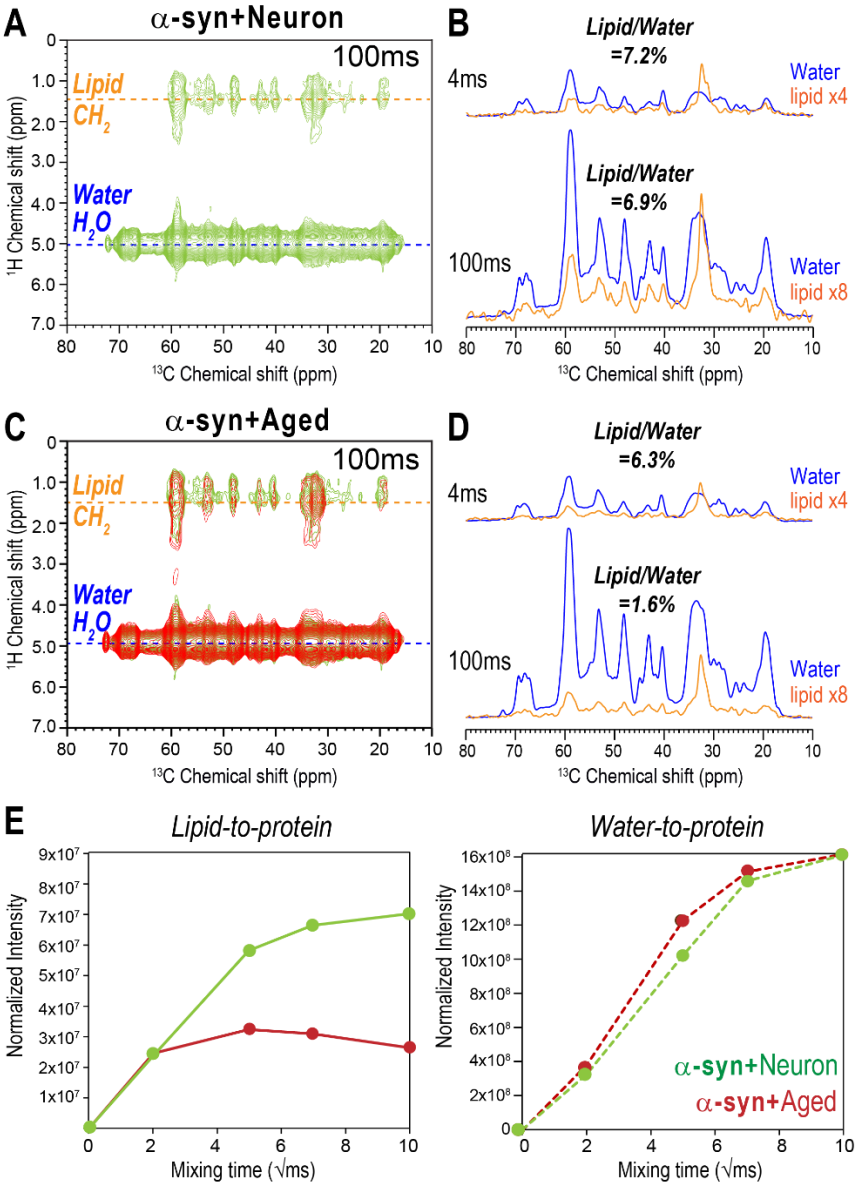

Figure 5. Membrane association of α-syn fibrils with Neuron and Aged membranes. (A, C) Representative 2D ^{1}H-^{13}C correlation spectra of α-syn fibrils grown with Neuron (A, green) and Aged membranes (C, red) at an L/P ratio of 10, measured with a ^{1}H mixing time of 100 ms. (B, D) ^{13}C cross sections at lipid CH_2 (1.3 ppm, orange) and water (5.0 ppm, blue) ^{1}H chemical shifts, extracted from 2D ^{1}H-^{13}C spectra of α-syn fibrils grown with Neuron (B) and Aged (D), measured at ^{1}H mixing times of 4 ms and 100 ms. The lipid cross-sections are scaled up by a factor of 4 or 8 relative to the water cross-section for clarity. At 100 ms, α-syn fibrils grown with Neuron membranes exhibit a higher lipid-to-protein cross peak intensity (7.2%) than those grown with Aged membranes (6.3%), suggesting stronger membrane interactions with Neuron membranes. (E) Lipid-to-protein (solid lines, left) and water-to-protein (dotted lines, right) ^{1}H polarization transfer curves as a function of ^{1}H mixing time. Protein signals transferred from Neuron membranes (green) continue to increase and are stronger than those from Aged membranes, indicating stronger α-syn fibril interactions with Neuron membranes.

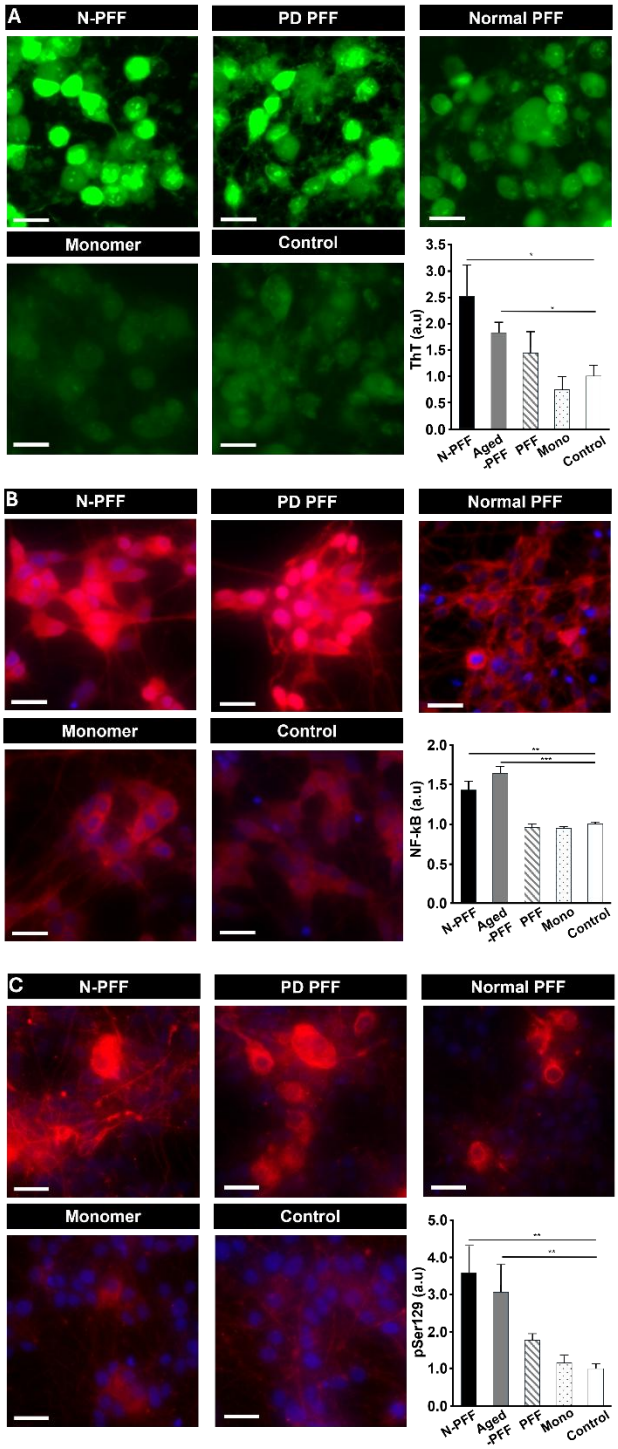

Figure 6. In vitro study on the pathological effects of polymorphic α-syn PFFs in dopaminergic neuronal cells. (A) Thioflavin T (ThT) fluorescence demonstrates distinct levels of α-syn aggregation templated by structurally different α-syn PFFs in dopaminergic neuronal cells. Scale bars, 20 µm. (B) Cells treated with different α-syn PFFs exhibit differential activation and nuclear translocation of NF-κB. Scale bars, 20 µm. (C) Immunostaining of phosphorylated α-syn (pSer129) shows varying levels of endogenous α-syn misfolding following treatments with conformationally distinct α-syn PFFs. Scale bars, 20 µm. ***$P < 0.001$, **$P < 0.01$, *$P < 0.05$. Data show mean ± SD with $n = 3$.

References

1. Calabresi, P., Mechelli, A., Natale, G., Volpicelli-Daley, L., Di Lazzaro, G., and Ghiglieri, V. (2023). Alpha-synuclein in Parkinson's disease and other synucleinopathies: from overt neurodegeneration back to early synaptic dysfunction. Cell Death Dis *14*, 176. 10.1038/s41419-023-05672-9.
2. Fusco, G., De Simone, A., Gopinath, T., Vostrikov, V., Vendruscolo, M., Dobson, C.M., and Veglia, G. (2014). Direct observation of the three regions in alpha-synuclein that determine its membrane-bound behaviour. Nat Commun *5*, 3827. 10.1038/ncomms4827.
3. Spillantini, M.G., Schmidt, M.L., Lee, V.M., Trojanowski, J.Q., Jakes, R., and Goedert, M. (1997). Alpha-synuclein in Lewy bodies. Nature *388*, 839-840. 10.1038/42166.
4. Spillantini, M.G., Crowther, R.A., Jakes, R., Hasegawa, M., and Goedert, M. (1998). alpha-Synuclein in filamentous inclusions of Lewy bodies from Parkinson's disease and dementia with lewy bodies. Proc Natl Acad Sci U S A *95*, 6469-6473. 10.1073/pnas.95.11.6469.
5. Wakabayashi, K., Yoshimoto, M., Tsuji, S., and Takahashi, H. (1998). Alpha-synuclein immunoreactivity in glial cytoplasmic inclusions in multiple system atrophy. Neurosci Lett *249*, 180-182. 10.1016/s0304-3940(98)00407-8.
6. Goldstein, D.S., Isonaka, R., Lamotte, G., and Kaufmann, H. (2021). Different phenoconversion pathways in pure autonomic failure with versus without Lewy bodies. Clin Auton Res *31*, 677-684. 10.1007/s10286-021-00829-y.
7. McKeith, I.G., Boeve, B.F., Dickson, D.W., Halliday, G., Taylor, J.P., Weintraub, D., Aarsland, D., Galvin, J., Attems, J., Ballard, C.G., et al. (2017). Diagnosis and management of dementia with Lewy bodies: Fourth consensus report of the DLB Consortium. Neurology *89*, 88-100. 10.1212/WNL.0000000000004058.
8. Krismer, F., and Wenning, G.K. (2017). Multiple system atrophy: insights into a rare and debilitating movement disorder. Nat Rev Neurol *13*, 232-243. 10.1038/nrneurol.2017.26.
9. Hoppe, S.O., Uzunoglu, G., and Nussbaum-Krammer, C. (2021). alpha-Synuclein Strains: Does Amyloid Conformation Explain the Heterogeneity of Synucleinopathies? Biomolecules *11*. 10.3390/biom11070931.
10. Mehra, S., Gadhe, L., Bera, R., Sawner, A.S., and Maji, S.K. (2021). Structural and Functional Insights into alpha-Synuclein Fibril Polymorphism. Biomolecules *11*. 10.3390/biom11101419.
11. Peng, C., Gathagan, R.J., Covell, D.J., Medellin, C., Stieber, A., Robinson, J.L., Zhang, B., Pitkin, R.M., Olufemi, M.F., Luk, K.C., et al. (2018). Cellular milieu imparts distinct pathological alpha-synuclein strains in alpha-synucleinopathies. Nature *557*, 558-563. 10.1038/s41586-018-0104-4.
12. Schmitz, M., Candelise, N., Canaslan, S., Altmeppen, H.C., Matschke, J., Glatzel, M., Younas, N., Zafar, S., Hermann, P., and Zerr, I. (2023). alpha-Synuclein conformers reveal link to clinical heterogeneity of alpha-synucleinopathies. Transl Neurodegener *12*, 12. 10.1186/s40035-023-00342-4.
13. Malfertheiner, K., Stefanova, N., and Heras-Garvin, A. (2021). The Concept of alpha-Synuclein Strains and How Different Conformations May Explain Distinct Neurodegenerative Disorders. Front Neurol *12*, 737195. 10.3389/fneur.2021.737195.
14. Sakalauskas, A., Ziaunys, M., and Smirnovas, V. (2019). Concentration-dependent polymorphism of insulin amyloid fibrils. PeerJ *7*, e8208. 10.7717/peerj.8208.
15. Ziaunys, M., Sakalauskas, A., Mikalauskaite, K., and Smirnovas, V. (2021). Polymorphism of Alpha-Synuclein Amyloid Fibrils Depends on Ionic Strength and Protein Concentration. Int J Mol Sci *22*. 10.3390/ijms222212382.
16. Chamachi, N.G., and Chakrabarty, S. (2017). Temperature-Induced Misfolding in Prion Protein: Evidence of Multiple Partially Disordered States Stabilized by Non-Native Hydrogen Bonds. Biochemistry *56*, 833-844. 10.1021/acs.biochem.6b01042.
17. Milto, K., Michailova, K., and Smirnovas, V. (2014). Elongation of mouse prion protein amyloid-like fibrils: effect of temperature and denaturant concentration. PLoS One *9*, e94469. 10.1371/journal.pone.0094469.

18. Tanaka, M., Chien, P., Yonekura, K., and Weissman, J.S. (2005). Mechanism of cross-species prion transmission: an infectious conformation compatible with two highly divergent yeast prion proteins. Cell *121*, 49-62. 10.1016/j.cell.2005.03.008.
19. Tao, Y., Sun, Y., Lv, S., Xia, W., Zhao, K., Xu, Q., Zhao, Q., He, L., Le, W., Wang, Y., et al. (2022). Heparin induces alpha-synuclein to form new fibril polymorphs with attenuated neuropathology. Nat Commun *13*, 4226. 10.1038/s41467-022-31790-7.
20. Arosio, P., Knowles, T.P., and Linse, S. (2015). On the lag phase in amyloid fibril formation. Phys Chem Chem Phys *17*, 7606-7618. 10.1039/c4cp05563b.
21. Pancoe, S.X., Wang, Y.J., Shimogawa, M., Perez, R.M., Giannakoulias, S., and Petersson, E.J. (2022). Effects of Mutations and Post-Translational Modifications on alpha-Synuclein In Vitro Aggregation. J Mol Biol *434*, 167859. 10.1016/j.jmb.2022.167859.
22. O'Leary, E.I., Jiang, Z., Strub, M.-P., and Lee, J.C. (2018). Effects of phosphatidylcholine membrane fluidity on the conformation and aggregation of N-terminally acetylated α-synuclein. J Biol Chem *293*, 11195-11205. 10.1074/jbc.RA118.002780.
23. Singh, B.P., Morris, R.J., Kunath, T., MacPhee, C.E., and Horrocks, M.H. (2023). Lipid-induced polymorphic amyloid fibril formation by alpha-synuclein. Protein Sci *32*, e4736. 10.1002/pro.4736.
24. Kurochka, A.S., Yushchenko, D.A., Bour, P., and Shvadchak, V.V. (2021). Influence of Lipid Membranes on alpha-Synuclein Aggregation. ACS Chem Neurosci *12*, 825-830. 10.1021/acschemneuro.0c00819.
25. Zhu, M., Li, J., and Fink, A.L. (2003). The association of alpha-synuclein with membranes affects bilayer structure, stability, and fibril formation. J Biol Chem *278*, 40186-40197. 10.1074/jbc.M305326200.
26. Mori, A., Imai, Y., and Hattori, N. (2020). Lipids: Key Players That Modulate alpha-Synuclein Toxicity and Neurodegeneration in Parkinson's Disease. Int J Mol Sci *21*. 10.3390/ijms21093301.
27. Makasewicz, K., Linse, S., and Sparr, E. (2024). Interplay of alpha-synuclein with Lipid Membranes: Cooperative Adsorption, Membrane Remodeling and Coaggregation. JACS Au *4*, 1250-1262. 10.1021/jacsau.3c00579.
28. Sharma, M., and Burre, J. (2023). alpha-Synuclein in synaptic function and dysfunction. Trends Neurosci *46*, 153-166. 10.1016/j.tins.2022.11.007.
29. Burre, J., Sharma, M., Tsetsenis, T., Buchman, V., Etherton, M.R., and Sudhof, T.C. (2010). Alpha-synuclein promotes SNARE-complex assembly in vivo and in vitro. Science *329*, 1663-1667. 10.1126/science.1195227.
30. Dixon, C., Mathias, N., Zweig, R.M., Davis, D.A., and Gross, D.S. (2005). Alpha-synuclein targets the plasma membrane via the secretory pathway and induces toxicity in yeast. Genetics *170*, 47-59. 10.1534/genetics.104.035493.
31. Shahmoradian, S.H., Lewis, A.J., Genoud, C., Hench, J., Moors, T.E., Navarro, P.P., Castano-Diez, D., Schweighauser, G., Graff-Meyer, A., Goldie, K.N., et al. (2019). Lewy pathology in Parkinson's disease consists of crowded organelles and lipid membranes. Nat Neurosci *22*, 1099-1109. 10.1038/s41593-019-0423-2.
32. Emamzadeh, F.N. (2016). Alpha-synuclein structure, functions, and interactions. J Res Med Sci *21*, 29. 10.4103/1735-1995.181989.
33. Ruf, V.C., Nübling, G.S., Willikens, S., Shi, S., Schmidt, F., Levin, J., Bötzel, K., Kamp, F., and Giese, A. (2019). Different Effects of α-Synuclein Mutants on Lipid Binding and Aggregation Detected by Single Molecule Fluorescence Spectroscopy and ThT Fluorescence-Based Measurements. ACS Chem Neurosci *10*, 1649-1659. 10.1021/acschemneuro.8b00579.
34. Galvagnion, C. (2017). The Role of Lipids Interacting with alpha-Synuclein in the Pathogenesis of Parkinson's Disease. J Parkinsons Dis *7*, 433-450. 10.3233/JPD-171103.
35. Galvagnion, C., Brown, J.W., Ouberai, M.M., Flagmeier, P., Vendruscolo, M., Buell, A.K., Sparr, E., and Dobson, C.M. (2016). Chemical properties of lipids strongly affect the kinetics of the membrane-induced aggregation of alpha-synuclein. Proc Natl Acad Sci U S A *113*, 7065-7070. 10.1073/pnas.1601899113.

36. Galvagnion, C., Buell, A.K., Meisl, G., Michaels, T.C., Vendruscolo, M., Knowles, T.P., and Dobson, C.M. (2015). Lipid vesicles trigger alpha-synuclein aggregation by stimulating primary nucleation. Nat Chem Biol *11*, 229-234. 10.1038/nchembio.1750.
37. Zhu, M., and Fink, A.L. (2003). Lipid binding inhibits alpha-synuclein fibril formation. J Biol Chem *278*, 16873-16877. 10.1074/jbc.M210136200.
38. Gaspar, R., Pallbo, J., Weininger, U., Linse, S., and Sparr, E. (2019). Reprint of "Ganglioside lipids accelerate alpha-synuclein amyloid formation". Biochim Biophys Acta Proteins Proteom *1867*, 508-518. 10.1016/j.bbapap.2019.02.003.
39. Watt, K.J.C., Meade, R.M., Williams, R.J., and Mason, J.M. (2022). Anionic lipid vesicles have differential effects on the aggregation of early onset-associated alpha-synuclein missense mutants. J Biol Chem *298*, 102565. 10.1016/j.jbc.2022.102565.
40. O'Leary, E.I., and Lee, J.C. (2019). Interplay between alpha-synuclein amyloid formation and membrane structure. Biochim Biophys Acta Proteins Proteom *1867*, 483-491. 10.1016/j.bbapap.2018.09.012.
41. Terakawa, M.S., Lee, Y.H., Kinoshita, M., Lin, Y., Sugiki, T., Fukui, N., Ikenoue, T., Kawata, Y., and Goto, Y. (2018). Membrane-induced initial structure of alpha-synuclein control its amyloidogenesis on model membranes. Biochim Biophys Acta Biomembr *1860*, 757-766. 10.1016/j.bbamem.2017.12.011.
42. Jiang, Z., de Messieres, M., and Lee, J.C. (2013). Membrane remodeling by alpha-synuclein and effects on amyloid formation. J Am Chem Soc *135*, 15970-15973. 10.1021/ja405993r.
43. Dasari, A.K.R., Dillard, L., Yi, S., Viverette, E., Hojjatian, A., Sengupta, U., Kayed, R., Taylor, K.A., Borgnia, M.J., and Lim, K.H. (2022). Untwisted alpha-Synuclein Filaments Formed in the Presence of Lipid Vesicles. Biochemistry *61*, 1766-1773. 10.1021/acs.biochem.2c00283.
44. Frieg, B., Antonschmidt, L., Dienemann, C., Geraets, J.A., Najbauer, E.E., Matthes, D., de Groot, B.L., Andreas, L.B., Becker, S., Griesinger, C., and Schroder, G.F. (2022). The 3D structure of lipidic fibrils of alpha-synuclein. Nat Commun *13*, 6810. 10.1038/s41467-022-34552-7.
45. Dou, T., Matveyenka, M., and Kurouski, D. (2023). Elucidation of Secondary Structure and Toxicity of alpha-Synuclein Oligomers and Fibrils Grown in the Presence of Phosphatidylcholine and Phosphatidylserine. ACS Chem Neurosci *14*, 3183-3191. 10.1021/acschemneuro.3c00314.
46. Zhaliazka, K., Ali, A., and Kurouski, D. (2024). Phospholipids and Cholesterol Determine Molecular Mechanisms of Cytotoxicity of alpha-Synuclein Oligomers and Fibrils. ACS Chem Neurosci *15*, 371-381. 10.1021/acschemneuro.3c00671.
47. Matveyenka, M., Zhaliazka, K., and Kurouski, D. (2023). Unsaturated fatty acids uniquely alter aggregation rate of alpha-synuclein and insulin and change the secondary structure and toxicity of amyloid aggregates formed in their presence. FASEB J *37*, e22972. 10.1096/fj.202300003R.
48. Antonschmidt, L., Dervisoglu, R., Sant, V., Tekwani Movellan, K., Mey, I., Riedel, D., Steinem, C., Becker, S., Andreas, L.B., and Griesinger, C. (2021). Insights into the molecular mechanism of amyloid filament formation: Segmental folding of alpha-synuclein on lipid membranes. Sci Adv *7*. 10.1126/sciadv.abg2174.
49. Norton, W.T., Abe, T., Poduslo, S.E., and DeVries, G.H. (1975). The lipid composition of isolated brain cells and axons. J Neurosci Res *1*, 57-75. 10.1002/jnr.490010106.
50. Giusto, N.M., Salvador, G.A., Castagnet, P.I., Pasquare, S.J., and Ilincheta de Boschero, M.G. (2002). Age-associated changes in central nervous system glycerolipid composition and metabolism. Neurochem Res *27*, 1513-1523. 10.1023/a:1021604623208.
51. Mota-Martorell, N., Andres-Benito, P., Martin-Gari, M., Galo-Licona, J.D., Sol, J., Fernandez-Bernal, A., Portero-Otin, M., Ferrer, I., Jove, M., and Pamplona, R. (2022). Selective brain regional changes in lipid profile with human aging. Geroscience *44*, 763-783. 10.1007/s11357-022-00527-1.
52. Pollard, A.K., Ortori, C.A., Stoger, R., Barrett, D.A., and Chakrabarti, L. (2017). Mouse mitochondrial lipid composition is defined by age in brain and muscle. Aging (Albany NY) *9*, 986-998. 10.18632/aging.101204.

53. Stephens, A.D., Matak-Vinkovic, D., Fernandez-Villegas, A., and Kaminski Schierle, G.S. (2020). Purification of Recombinant alpha-synuclein: A Comparison of Commonly Used Protocols. Biochemistry *59*, 4563-4572. 10.1021/acs.biochem.0c00725.
54. Takegoshi, K., Nakamura, S., and Terao, T. (2001). 13C-1H dipolar-assisted rotational resonance in magic-angle spinning NMR. Chem. Phys. Lett *344*, 631-637.
55. Morcombe, C.R., Gaponenko, V., Byrd, R.A., and Zilm, K.W. (2004). Diluting abundant spins by isotope edited radio frequency field assisted diffusion. J Am Chem Soc *126*, 7196-7197. 10.1021/ja047919t.
56. Huster, D., Yao, X., and Hong, M. (2002). Membrane protein topology probed by (1)H spin diffusion from lipids using solid-state NMR spectroscopy. J Am Chem Soc *124*, 874-883. 10.1021/ja017001r.
57. Kumashiro, K.K., Schmidt-Rohr, K., Murphy, O.J., Ouellette, K.L., Cramer, W.A., and Thompson, L.K. (1998). A Novel Tool for Probing Membrane Protein Structure: Solid-State NMR with Proton Spin Diffusion and X-Nucleus Detection. J Am Chem Soc *120*, 5043-5051. 10.1021/ja972655e.
58. Dutta, S., Watson, B.G., Mattoo, S., and Rochet, J.C. (2020). Calcein Release Assay to Measure Membrane Permeabilization by Recombinant Alpha-Synuclein. Bio Protoc *10*. 10.21769/bioprotoc.3690.
59. Georgieva, E.R., Ramlall, T.F., Borbat, P.P., Freed, J.H., and Eliezer, D. (2008). Membrane-bound alpha-synuclein forms an extended helix: long-distance pulsed ESR measurements using vesicles, bicelles, and rodlike micelles. J Am Chem Soc *130*, 12856-12857. 10.1021/ja804517m.
60. Ferreon, A.C., Gambin, Y., Lemke, E.A., and Deniz, A.A. (2009). Interplay of alpha-synuclein binding and conformational switching probed by single-molecule fluorescence. Proc Natl Acad Sci U S A *106*, 5645-5650. 10.1073/pnas.0809232106.
61. Ulmer, T.S., and Bax, A. (2005). Comparison of structure and dynamics of micelle-bound human alpha-synuclein and Parkinson disease variants. J Biol Chem *280*, 43179-43187. 10.1074/jbc.M507624200.
62. Kwon, B., Lee, M., Waring, A.J., and Hong, M. (2018). Oligomeric Structure and Three-Dimensional Fold of the HIV gp41 Membrane-Proximal External Region and Transmembrane Domain in Phospholipid Bilayers. J Am Chem Soc *140*, 8246-8259. 10.1021/jacs.8b04010.
63. Lee, M., Morgan, C.A., and Hong, M. (2019). Fully hydrophobic HIV gp41 adopts a hemifusion-like conformation in phospholipid bilayers. J Biol Chem *294*, 14732-14744. 10.1074/jbc.RA119.009542.
64. Yao, H., Lee, M.W., Waring, A.J., Wong, G.C., and Hong, M. (2015). Viral fusion protein transmembrane domain adopts beta-strand structure to facilitate membrane topological changes for virus-cell fusion. Proc Natl Acad Sci U S A *112*, 10926-10931. 10.1073/pnas.1501430112.
65. Kamath, T., Abdulraouf, A., Burris, S.J., Langlieb, J., Gazestani, V., Nadaf, N.M., Balderrama, K., Vanderburg, C., and Macosko, E.Z. (2022). Single-cell genomic profiling of human dopamine neurons identifies a population that selectively degenerates in Parkinson's disease. Nat Neurosci *25*, 588-595. 10.1038/s41593-022-01061-1.
66. Michel, P.P., Hirsch, E.C., and Hunot, S. (2016). Understanding Dopaminergic Cell Death Pathways in Parkinson Disease. Neuron *90*, 675-691. 10.1016/j.neuron.2016.03.038.
67. Lo Bianco, C., Ridet, J.L., Schneider, B.L., Deglon, N., and Aebischer, P. (2002). alpha -Synucleinopathy and selective dopaminergic neuron loss in a rat lentiviral-based model of Parkinson's disease. Proc Natl Acad Sci U S A *99*, 10813-10818. 10.1073/pnas.152339799.
68. Ioghen, O.C., Ceafalan, L.C., and Popescu, B.O. (2023). SH-SY5Y Cell Line In Vitro Models for Parkinson Disease Research-Old Practice for New Trends. J Integr Neurosci *22*, 20. 10.31083/j.jin2201020.
69. Xicoy, H., Wieringa, B., and Martens, G.J. (2017). The SH-SY5Y cell line in Parkinson's disease research: a systematic review. Mol Neurodegener *12*, 10. 10.1186/s13024-017-0149-0.
70. Xie, H.R., Hu, L.S., and Li, G.Y. (2010). SH-SY5Y human neuroblastoma cell line: in vitro cell model of dopaminergic neurons in Parkinson's disease. Chin Med J (Engl) *123*, 1086-1092.
71. Dravid, A., Raos, B., Svirskis, D., and O'Carroll, S.J. (2021). Optimised techniques for high-throughput screening of differentiated SH-SY5Y cells and application for neurite outgrowth assays. Sci Rep *11*, 23935. 10.1038/s41598-021-03442-1.

72. Shipley, M.M., Mangold, C.A., and Szpara, M.L. (2016). Differentiation of the SH-SY5Y Human Neuroblastoma Cell Line. J Vis Exp, 53193. 10.3791/53193.
73. Soltani, M.H., Pichardo, R., Song, Z., Sangha, N., Camacho, F., Satyamoorthy, K., Sangueza, O.P., and Setaluri, V. (2005). Microtubule-associated protein 2, a marker of neuronal differentiation, induces mitotic defects, inhibits growth of melanoma cells, and predicts metastatic potential of cutaneous melanoma. Am J Pathol *166*, 1841-1850. 10.1016/s0002-9440(10)62493-5.
74. Harada, A., Teng, J., Takei, Y., Oguchi, K., and Hirokawa, N. (2002). MAP2 is required for dendrite elongation, PKA anchoring in dendrites, and proper PKA signal transduction. J Cell Biol *158*, 541-549. 10.1083/jcb.200110134.
75. Okada, M., Kawagoe, Y., Sato, Y., Nozumi, M., Ishikawa, Y., Tamada, A., Yamazaki, H., Sekino, Y., Kanemura, Y., Shinmyo, Y., et al. (2021). Phosphorylation of GAP-43 T172 is a molecular marker of growing axons in a wide range of mammals including primates. Mol Brain *14*, 66. 10.1186/s13041-021-00755-0.
76. Denny, J.B. (2006). Molecular mechanisms, biological actions, and neuropharmacology of the growth-associated protein GAP-43. Curr Neuropharmacol *4*, 293-304. 10.2174/157015906778520782.
77. Skene, J.H. (1989). Axonal growth-associated proteins. Annu Rev Neurosci *12*, 127-156. 10.1146/annurev.ne.12.030189.001015.
78. Weihe, E., Depboylu, C., Schütz, B., Schäfer, M.K., and Eiden, L.E. (2006). Three types of tyrosine hydroxylase-positive CNS neurons distinguished by dopa decarboxylase and VMAT2 co-expression. Cell Mol Neurobiol *26*, 659-678. 10.1007/s10571-006-9053-9.
79. White, R.B., and Thomas, M.G. (2012). Moving beyond tyrosine hydroxylase to define dopaminergic neurons for use in cell replacement therapies for Parkinson's disease. CNS Neurol Disord Drug Targets *11*, 340-349. 10.2174/187152712800792758.
80. Kim, B.J., Noh, H.R., Jeon, H., and Park, S.M. (2023). Monitoring α-synuclein Aggregation Induced by Preformed α-synuclein Fibrils in an In Vitro Model System. Exp Neurobiol *32*, 147-156. 10.5607/en23007.
81. Cascella, R., Chen, S.W., Bigi, A., Camino, J.D., Xu, C.K., Dobson, C.M., Chiti, F., Cremades, N., and Cecchi, C. (2021). The release of toxic oligomers from alpha-synuclein fibrils induces dysfunction in neuronal cells. Nat Commun *12*, 1814. 10.1038/s41467-021-21937-3.
82. Bigi, A., Ermini, E., Chen, S.W., Cascella, R., and Cecchi, C. (2021). Exploring the Release of Toxic Oligomers from α-Synuclein Fibrils with Antibodies and STED Microscopy. Life (Basel) *11*. 10.3390/life11050431.
83. Feng, C., Flores, M., Dhoj, C., Garcia, A., Belleca, S., Abbas, D.A., Parres-Gold, J., Anguiano, A., Porter, E., and Wang, Y. (2022). Observation of α-Synuclein Preformed Fibrils Interacting with SH-SY5Y Neuroblastoma Cell Membranes Using Scanning Ion Conductance Microscopy. ACS Chem Neurosci *13*, 3547-3553. 10.1021/acschemneuro.2c00478.
84. Feller, B., Fallon, A., Luo, W., Nguyen, P.T., Shlaifer, I., Lee, A.K., Chofflet, N., Yi, N., Khaled, H., Karkout, S., et al. (2023). α-Synuclein Preformed Fibrils Bind to β-Neurexins and Impair β-Neurexin-Mediated Presynaptic Organization. Cells *12*. 10.3390/cells12071083.
85. Ghanem, S.S., Majbour, N.K., Vaikath, N.N., Ardah, M.T., Erskine, D., Jensen, N.M., Fayyad, M., Sudhakaran, I.P., Vasili, E., Melachroinou, K., et al. (2022). α-Synuclein phosphorylation at serine 129 occurs after initial protein deposition and inhibits seeded fibril formation and toxicity. Proc Natl Acad Sci U S A *119*, e2109617119. 10.1073/pnas.2109617119.
86. Guan, Y., Zhao, X., Liu, F., Yan, S., Wang, Y., Du, C., Cui, X., Li, R., and Zhang, C.X. (2020). Pathogenic Mutations Differentially Regulate Cell-to-Cell Transmission of α-Synuclein. Front Cell Neurosci *14*, 159. 10.3389/fncel.2020.00159.
87. Biancalana, M., and Koide, S. (2010). Molecular mechanism of Thioflavin-T binding to amyloid fibrils. Biochim Biophys Acta *1804*, 1405-1412. 10.1016/j.bbapap.2010.04.001.
88. Lema Tomé, C.M., Tyson, T., Rey, N.L., Grathwohl, S., Britschgi, M., and Brundin, P. (2013). Inflammation and α-synuclein's prion-like behavior in Parkinson's disease--is there a link? Mol Neurobiol *47*, 561-574. 10.1007/s12035-012-8267-8.

89. Cardinale, A., Calabrese, V., de Iure, A., and Picconi, B. (2021). Alpha-Synuclein as a Prominent Actor in the Inflammatory Synaptopathy of Parkinson's Disease. Int J Mol Sci *22*. 10.3390/ijms22126517.
90. Gao, H.M., Kotzbauer, P.T., Uryu, K., Leight, S., Trojanowski, J.Q., and Lee, V.M. (2008). Neuroinflammation and oxidation/nitration of alpha-synuclein linked to dopaminergic neurodegeneration. J Neurosci *28*, 7687-7698. 10.1523/jneurosci.0143-07.2008.
91. Shih, R.H., Wang, C.Y., and Yang, C.M. (2015). NF-kappaB Signaling Pathways in Neurological Inflammation: A Mini Review. Front Mol Neurosci *8*, 77. 10.3389/fnmol.2015.00077.
92. Singh, S.S., Rai, S.N., Birla, H., Zahra, W., Rathore, A.S., and Singh, S.P. (2020). NF-κB-Mediated Neuroinflammation in Parkinson's Disease and Potential Therapeutic Effect of Polyphenols. Neurotox Res *37*, 491-507. 10.1007/s12640-019-00147-2.
93. Wang, Y., Shi, M., Chung, K.A., Zabetian, C.P., Leverenz, J.B., Berg, D., Srulijes, K., Trojanowski, J.Q., Lee, V.M., Siderowf, A.D., et al. (2012). Phosphorylated α-synuclein in Parkinson's disease. Sci Transl Med *4*, 121ra120. 10.1126/scitranslmed.3002566.
94. Chen, L., Periquet, M., Wang, X., Negro, A., McLean, P.J., Hyman, B.T., and Feany, M.B. (2009). Tyrosine and serine phosphorylation of alpha-synuclein have opposing effects on neurotoxicity and soluble oligomer formation. J Clin Invest *119*, 3257-3265. 10.1172/jci39088.
95. Fujiwara, H., Hasegawa, M., Dohmae, N., Kawashima, A., Masliah, E., Goldberg, M.S., Shen, J., Takio, K., and Iwatsubo, T. (2002). alpha-Synuclein is phosphorylated in synucleinopathy lesions. Nat Cell Biol *4*, 160-164. 10.1038/ncb748.
96. Grey, M., Dunning, C.J., Gaspar, R., Grey, C., Brundin, P., Sparr, E., and Linse, S. (2015). Acceleration of alpha-synuclein aggregation by exosomes. J Biol Chem *290*, 2969-2982. 10.1074/jbc.M114.585703.
97. Bigay, J., and Antonny, B. (2012). Curvature, lipid packing, and electrostatics of membrane organelles: defining cellular territories in determining specificity. Dev Cell *23*, 886-895. 10.1016/j.devcel.2012.10.009.
98. Nuscher, B., Kamp, F., Mehnert, T., Odoy, S., Haass, C., Kahle, P.J., and Beyer, K. (2004). Alpha-synuclein has a high affinity for packing defects in a bilayer membrane: a thermodynamics study. J Biol Chem *279*, 21966-21975. 10.1074/jbc.M401076200.
99. Ouberai, M.M., Wang, J., Swann, M.J., Galvagnion, C., Guilliams, T., Dobson, C.M., and Welland, M.E. (2013). alpha-Synuclein senses lipid packing defects and induces lateral expansion of lipids leading to membrane remodeling. J Biol Chem *288*, 20883-20895. 10.1074/jbc.M113.478297.
100. Johnson, D.H., Kou, O.H., White, J.M., Ramirez, S.Y., Margaritakis, A., Chung, P.J., Jaeger, V.W., and Zeno, W.F. (2025). Lipid packing defects are necessary and sufficient for membrane binding of alpha-synuclein. Commun Biol *8*, 1179. 10.1038/s42003-025-08622-7.
101. Qi, Z., Wan, M., Zhang, J., and Li, Z. (2023). Influence of Cholesterol on the Membrane Binding and Conformation of alpha-Synuclein. J Phys Chem B *127*, 1956-1964. 10.1021/acs.jpcb.2c08077.
102. Tuttle, M.D., Comellas, G., Nieuwkoop, A.J., Covell, D.J., Berthold, D.A., Kloepper, K.D., Courtney, J.M., Kim, J.K., Barclay, A.M., Kendall, A., et al. (2016). Solid-state NMR structure of a pathogenic fibril of full-length human alpha-synuclein. Nat Struct Mol Biol *23*, 409-415. 10.1038/nsmb.3194.
103. Middleton, E.R., and Rhoades, E. (2010). Effects of curvature and composition on alpha-synuclein binding to lipid vesicles. Biophys J *99*, 2279-2288. 10.1016/j.bpj.2010.07.056.
104. Jo, E., Fuller, N., Rand, R.P., St George-Hyslop, P., and Fraser, P.E. (2002). Defective membrane interactions of familial Parkinson's disease mutant A30P alpha-synuclein. J Mol Biol *315*, 799-807. 10.1006/jmbi.2001.5269.
105. Lau, A., So, R.W.L., Lau, H.H.C., Sang, J.C., Ruiz-Riquelme, A., Fleck, S.C., Stuart, E., Menon, S., Visanji, N.P., Meisl, G., et al. (2020). alpha-Synuclein strains target distinct brain regions and cell types. Nat Neurosci *23*, 21-31. 10.1038/s41593-019-0541-x.
106. Rey, N.L., Bousset, L., George, S., Madaj, Z., Meyerdirk, L., Schulz, E., Steiner, J.A., Melki, R., and Brundin, P. (2019). alpha-Synuclein conformational strains spread, seed and target neuronal cells differentially after injection into the olfactory bulb. Acta Neuropathol Commun *7*, 221. 10.1186/s40478-019-0859-3.

107. Guerrero-Ferreira, R., Taylor, N.M., Arteni, A.A., Kumari, P., Mona, D., Ringler, P., Britschgi, M., Lauer, M.E., Makky, A., Verasdonck, J., et al. (2019). Two new polymorphic structures of human full-length alpha-synuclein fibrils solved by cryo-electron microscopy. Elife *8*. 10.7554/eLife.48907.
108. Guerrero-Ferreira, R., Taylor, N.M., Mona, D., Ringler, P., Lauer, M.E., Riek, R., Britschgi, M., and Stahlberg, H. (2018). Cryo-EM structure of alpha-synuclein fibrils. Elife *7*. 10.7554/eLife.36402.
109. Li, Y., Zhao, C., Luo, F., Liu, Z., Gui, X., Luo, Z., Zhang, X., Li, D., Liu, C., and Li, X. (2018). Amyloid fibril structure of alpha-synuclein determined by cryo-electron microscopy. Cell Res *28*, 897-903. 10.1038/s41422-018-0075-x.
110. Spillantini, M.G., and Goedert, M. (2000). The alpha-synucleinopathies: Parkinson's disease, dementia with Lewy bodies, and multiple system atrophy. Ann N Y Acad Sci *920*, 16-27. 10.1111/j.1749-6632.2000.tb06900.x.
111. Melki, R. (2015). Role of Different Alpha-Synuclein Strains in Synucleinopathies, Similarities with other Neurodegenerative Diseases. J Parkinsons Dis *5*, 217-227. 10.3233/jpd-150543.
112. Rey, N.L., Steiner, J.A., Maroof, N., Luk, K.C., Madaj, Z., Trojanowski, J.Q., Lee, V.M., and Brundin, P. (2016). Widespread transneuronal propagation of α-synucleinopathy triggered in olfactory bulb mimics prodromal Parkinson's disease. J Exp Med *213*, 1759-1778. 10.1084/jem.20160368.
113. Mezias, C., Rey, N., Brundin, P., and Raj, A. (2020). Neural connectivity predicts spreading of alpha-synuclein pathology in fibril-injected mouse models: Involvement of retrograde and anterograde axonal propagation. Neurobiol Dis *134*, 104623. 10.1016/j.nbd.2019.104623.
114. Kulkarni, A.S., Burns, M.R., Brundin, P., and Wesson, D.W. (2022). Linking α-synuclein-induced synaptopathy and neural network dysfunction in early Parkinson's disease. Brain Commun *4*, fcac165. 10.1093/braincomms/fcac165.